PROGRAM IN SUPPORT OF THE JUMPER PROGRAM FOR LASER ISOTOPE SEPARATION

Alan L. McWhorter

Massachusetts Institute of Technology

Prepared for:

Electronic Systems Division

31 December 1975

MASSACHUSETTS INSTITUTE OF TECHNOLOGY
LINCOLN LABORATORY

PROGRAM IN SUPPORT OF THE JUMPER PROGRAM FOR LASER ISOTOPE SEPARATION

SEMIANNUAL REPORT

1 JULY – 31 DECEMBER 1975

ISSUED 23 JANUARY 1976

Submitted to
Los Alamos Scientific Laboratory

LEXINGTON MASSACHUSETTS

ABSTRACT

This report covers in detail the research and development work carried out by M.I.T. Lincoln Laboratory for the U.S. Energy Research and Development Administration under subcontract from the Los Alamos Scientific Laboratory as part of the JUMPer program during the period 1 July through 31 December 1975. The topics covered include infrared nonlinear crystal growth, evaluation, and application; optically pumped gas laser research; and stable CO_2 laser development.

CONTENTS

INTRODUCTION

Over 60 ingots of $CdGeAs_2$ have been grown during the reporting period. The material was dominantly p-type and the yield of usable single crystals of volumes of at least 1 cm^3 has been increased.

The optical absorption in $CdGeAs_2$ has been tentatively shown not to arise from foreign impurities. It has been found, however, that the strength of the optical absorption increases with hole concentration. Electrical measurements show considerable spatial variation in hole concentration and a donor-acceptor model has been developed which correlates well with the observed temperature dependences in the electrical data.

Seeded Bridgman growth of $AgGaSe_2$ has been demonstrated. By optimizing the amount of excess Se and Ag it should be possible to minimize precipitates and make high optical quality material.

Second harmonic generation in $CdGeAs_2$ of radiation from cw and high repetition rate Q-switched CO_2 lasers has been studied. Efficiencies for cw and Q-switched operation have been observed to be 0.5% and 18% respectively. Using a repetitively pulsed TEA laser the limits of high peak/high average power operation are being explored. Average powers of 0.31 W were obtained at 50 Hz (6.2 mJ/pulse) during the first minute of operation. The power subsequently dropped indicating heating effects.

Phasematching angles have been measured at liquid nitrogen temperature for difference frequency generation between 12.3 and 15.7 μm using CO_2 and CO lasers. The observed difference between 300 K and 80 K is within the experimental uncertainty in crystal orientation and boule-to-boule variations in phasematching angles.

A SiH_4 laser has been operated and is the first example of optically pumped transfer laser action in a nonlinear molecule. The optical gain decreases with pressure and the laser ceases operation at 35 Torr. Six SiH_4 lines have been observed in the 7.90-7.99-μm region.

The high-pressure limit for laser operation in C_2H_2-CO-He and OCS-CO-He has been studied. The threshold pump power increases linearly with pressure until the pump pulse length becomes comparable with the deactivation time after which the power required has an apparent exponential dependence on pressure. Acetylene has been operated at pressures up to 610 Torr and a 3% slope efficiency was obtained using a 1:3:30 mixture of C_2H_2-CO-He.

In related work supported by the U. S. Air Force a 16 atm CO_2-CO transfer laser has been operated and experiments are underway to demonstrate continuous tuning at high average powers.

A grating-tuned $O^{12}CS$ laser has been developed. $O^{13}CS$ was also operated as a laser, but with the available pump energies grating-tuned operation was marginal.

A 16 μm CO_2 laser has been constructed using a mixture of CO_2 and HBr pumped by HBr and CO_2 lasers. A number of experiments have been performed which demonstrate the relative importance of various kinetic rates and show that pressure scaling is possible. A high-pressure (100 Torr), room temperature operation has been obtained using a high energy CO_2-TEA laser (TAC 2).

Tunable diode laser measurements of $^{14}NH_3$ and $^{15}NH_3$ have been made in the 12.2 μm region. The diode laser data as well as LASL data have been compared with data from Rao and a number of lines identified. The frequency of a $^{14}C^{16}O_2$ laser transition was measured, using heterodyne techniques, relative to an ammonia line providing a calibration accuracy of ± 0.002 cm^{-1}.

In work jointly supported by LASL and the U. S. Air Force, an ultrastable, high repetition rate, passively Q-switched CO_2 laser system has been operated. With SF_6 as the Q-switch, repetition rates from 10 kHz to 150 kHz were observed.

1. GROWTH AND CHARACTERIZATION OF NONLINEAR OPTICAL CRYSTALS

1.1 $CdGeAs_2$

We have grown more than 60 ingots of $CdGeAs_2$ in the six month period covered in this report. Many of these ingots contain only one or two grain boundaries and the yield of single crystal and uncracked pieces with volumes of at least 1 cm^3 has increased. Nearly all of the material is p-type with carrier concentration ranging from 1.4×10^{15} to about 2×10^{16} cm^{-3} at room temperature. One sample was particularly interesting because it exhibited the lowest hole concentration at room temperature that we have observed to date, 1.4×10^{15} cm^{-3}, and also the lowest absorption constants at the wavelengths of interest to LASL, namely 0.95 cm^{-1} at 5 μm, 0.25 cm^{-1} at 10 μm and 0.8 cm^{-1} at 16 μm, all at room temperature.

We believe that we have made some progress toward the goal of understanding the cause of the optical absorption that is so troublesome at 5 μm and in some crystals at 10 μm and beyond. In three separate experiments, the reacted compound was zone refined with at least 35 zone passes prior to growth to try to remove impurities which might induce the absorption. No improvement in the optical properties was observed, however, for samples of the three ingots grown from the zone refined material. Based on these experiments and on many mass spectrographic analyses, we have reached the very tentative conclusion that large foreign impurity concentrations probably are not responsible for the broad optical absorption extending from the band edge out to beyond 10 μm. We will not spend more time on zone refining during the next quarter.

Another observation which we have made is that the strength of the optical absorption increases with the hole concentration. Hole mobilities vary widely from sample to sample but there appears to be no correlation between mobility and absorption coefficient. Some of our data are shown in Fig. 1.1-1 where the absorption constant at 5 μm both for 80 and 300 K is plotted versus room temperature

hole concentration for samples grown during this report period. Electrical and optical measurements were made on the same samples in most cases; in the others, two samples from near neighbor slices of an ingot were used. The large error bars on the carrier concentrations represent the values obtained from two sets of electrical leads for the Hall measurements on each sample. The hole concentration is clearly very nonuniform since the two sets of Hall leads are separated by only about 4 mm on most samples and over this short distance factors of 5 variation in hole concentration are often observed. Although no error bars are indicated for the absorption constants, they too are very uncertain due to optical nonuniformity. The sample with the highest absorption constant and highest carrier concentration was grown from a melt of composition, $CdGe_{1.025}As_2$, and all of the others were grown from melts with the three elements in their stoichiometric ratios. While the scatter in the data is very large, it is clear that the absorption coefficient at 5 μm both at 80 and 300 K increases with increasing room temperature hole concentration. (There is no correlation between the absorption strength at 80 or 300 K with the carrier concentration at 80 K; we will return to this point later in the text.) These data indicate that p-type crystals with hole concentrations of 10^{15} cm^{-3} or less would be quite adequate for infrared mixing to obtain the 16 μm radiation which LASL requires. Absorption spectra at 300 and 80 K for a sample with 1.4×10^{15} holes per cm^3 at room temperature are shown in Fig. 1.1-2. Even for this low carrier concentration, there is much less absorption at 80 than at 300 K. Note that the absorption constant changes from about 0.95 to 0.4 cm^{-1} at 5 μm, from 0.25 to 0.09 cm^{-1} at 10 μm and from 0.8 to 0.2 cm^{-1} at 16 μm on cooling from room temperature to liquid nitrogen.

In a further effort to understand the nature of the absorption, we have made Hall and resistivity measurements as a function of temperature for temperatures between 80 and 375 K. Some of our resistivity data are shown in Fig. 1.1-3 where

resistivity is plotted on a log scale versus reciprocal temperature, for 5 samples. The resistivity increases rapidly as the temperature is reduced, due to carrier freeze-out onto deep acceptor levels. Each resistivity reaches a nearly constant, but different value when the temperature is reduced sufficiently.

The Hall constant is plotted in Fig. 1.1-4 on a log scale as a function of reciprocal temperature for the sample with the highest resistivity on the previous figure. For temperatures less than 300 K, the same type of behavior is observed as for the resistivity, because the hole mobility does not change very rapidly with temperature. At temperatures greater than 300 K, carriers are thermally excited across the band gap and the Hall constant becomes negative above 345 K because the electron mobility is larger than the hole mobility. On cooling below 125 K, not much more change in hole concentration occurs. Any model to explain these data should contain at least three kinds of electrically active defect and/or impurity centers. Deep acceptors must exist for the holes to deionize from about 125 to 80 K. Because the hole mobilities are quite low (100-200 with a rare 400 cm^2/volt-sec at 300 K) we also postulate the presence of donor levels. For such a model, the value of the carrier concentration at the lowest temperature shown is equal to the shallow acceptor concentration, N_{A1}, minus the donor concentration, N_D; the difference is 4.2×10^{11} cm^{-3} for this sample. The slope of the straight line segment of the curve between about 300 and 150 K gives a deep acceptor ionization energy of 0.3 eV. The hole and electron effective masses are approximately 0.26 and 0.035[1.1-1] and the energy gap is about 0.55 eV[1.1-2] between 300 and 400 K. Using these parameters one can fit the Hall data quite well as shown by the solid curve in Fig. 1.1-4 by choosing 5×10^{16} cm^{-3} for the deep acceptor concentration, N_{A2}, and 25 for the mobility ratio. Estimates for the values of N_D or N_{A1} are not possible from these data. The surprising result is that the acceptor level is deep and about 0.3 eV from the valence band edge and also nearly 0.3 eV from the conduction

band edge. Therefore optical absorption due to transitions to or from this level could not extend beyond about 4 μm in wavelength. The residual absorption that we observe at 300 K all the way out to 15 μm may be due to intervalence band transitions,[1.1-3] perhaps at more than one point in the Brillouin zone. The absorption at wavelengths less than 4 μm does not decrease much with decreasing temperature, as seen in Fig. 1.1-2. It may be due to transitions from the valence band to the deep acceptors and from the deep acceptors to the valence band. The absorption strength of the first process increases with decreasing temperature while that of the second decreases and the net could be nearly temperature independent, as observed.

It is interesting that the difference of the donor concentration and the shallow acceptor concentration is as small as 4.2×10^{11} cm^{-3} for the sample of Fig. 1.1-4. This difference is not so low for all samples (note the various values at which the resistivity curves become flat in Fig. 1.1-3) but it is usually less than 10^{14} cm^{-3}. As mentioned above there is no obvious correlation between this difference, which is equal to the carrier concentration at 80 K, and the optical transmission of the crystals. Presumably some compensation mechanism fixes N_D at a value very close to that of N_{Al}. We have never observed a p-type sample for which $N_D > N_{Al}$ but we will try to diffuse a donor, such as In or Sc, into some crystals in the next quarter to reduce the carrier concentrations. Diffusion coefficients for Cd, Ge and As must be quite small because we have annealed 1 mm thick samples for 2 weeks at 600°C in atmospheres of Cd and Ge or As and have not been able to change the carrier concentration at all. n-type crystals grown to date have all exhibited carrier concentrations in excess of 2×10^{17} cm^{-3}, whether doped or undoped, and they have all been more opaque than our worst p-type samples.

During the next quarter we will continue our effort to optimize the growth conditions for a better yield of high quality crystals. As mentioned above, some

diffusion experiments will be undertaken and we will continue to study any properties which can lead to a better understanding of the problems associated with producing $CdGeAs_2$ crystals suitable for nonlinear infrared mixing.

G. W. Iseler
H. Kildal

References:

1.1-1 H. Kildal, Technical Report AFML-TR-72-277.

1.1-2 A. Shileika, Surf. Sci. 37, 730 (1973).

1.1-3 H. Kildal, Phys. Rev. B 10, 5082 (1974).

Figure Captions:

1.1-1 Absorption constants at 5 μm both at 80 and 300 K versus room temperature hole concentration for $CdGeAs_2$ crystals.

1.1-2 Absorption spectra at 80 and 300 K for a $CdGeAs_2$ sample with 1.4×10^{15} holes per cm^3 at room temperature.

1.1-3 Resistivity versus reciprocal temperature for five $CdGeAs_2$ samples.

1.1-4 Hall constant versus reciprocal temperature for the $CdGeAs_2$ sample whose absorption spectra are shown in Fig. 1.1-2. The solid line was calculated from the model and parameters discussed in the text.

18-8-13232

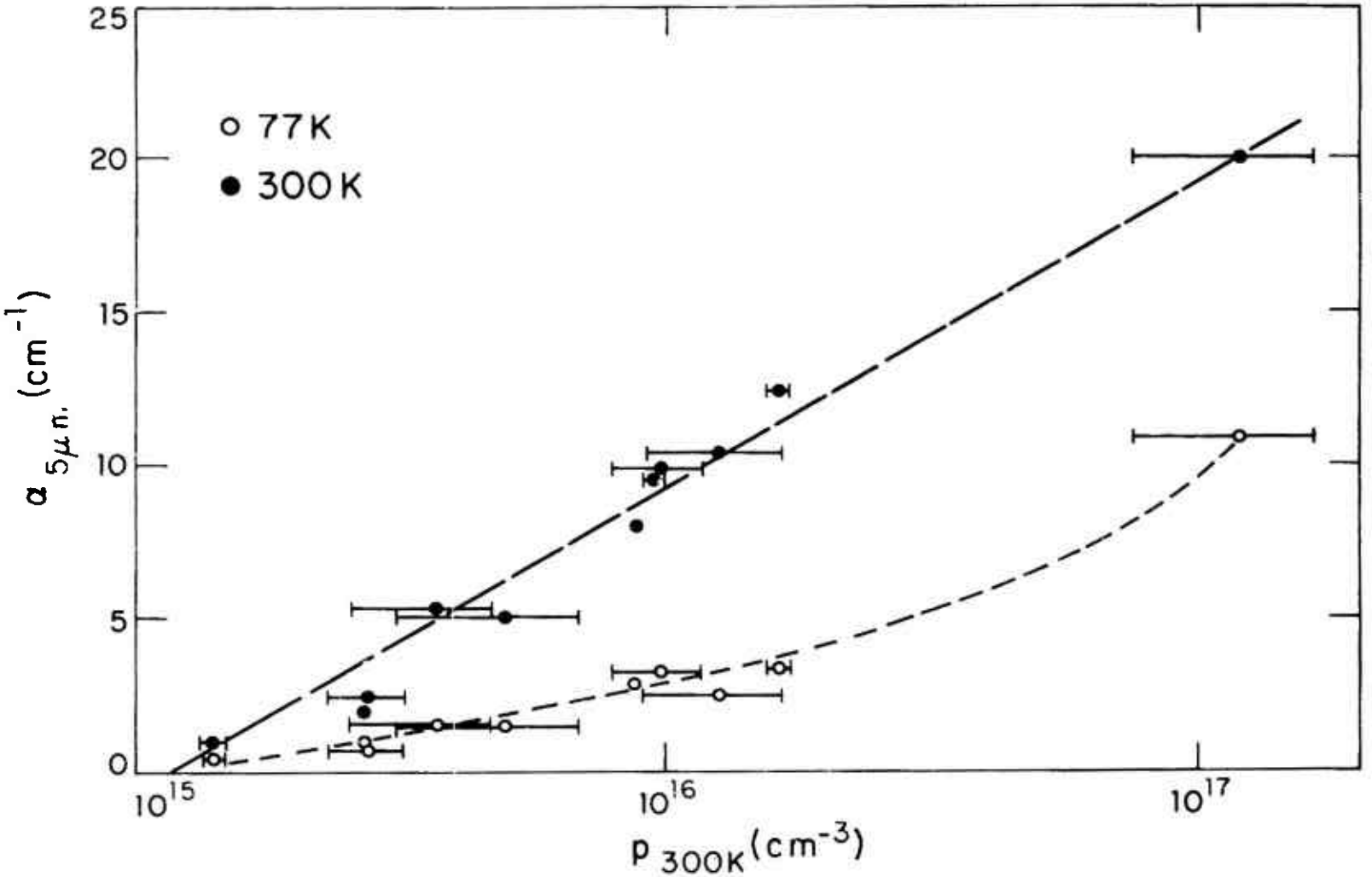

Fig. 1.1-1

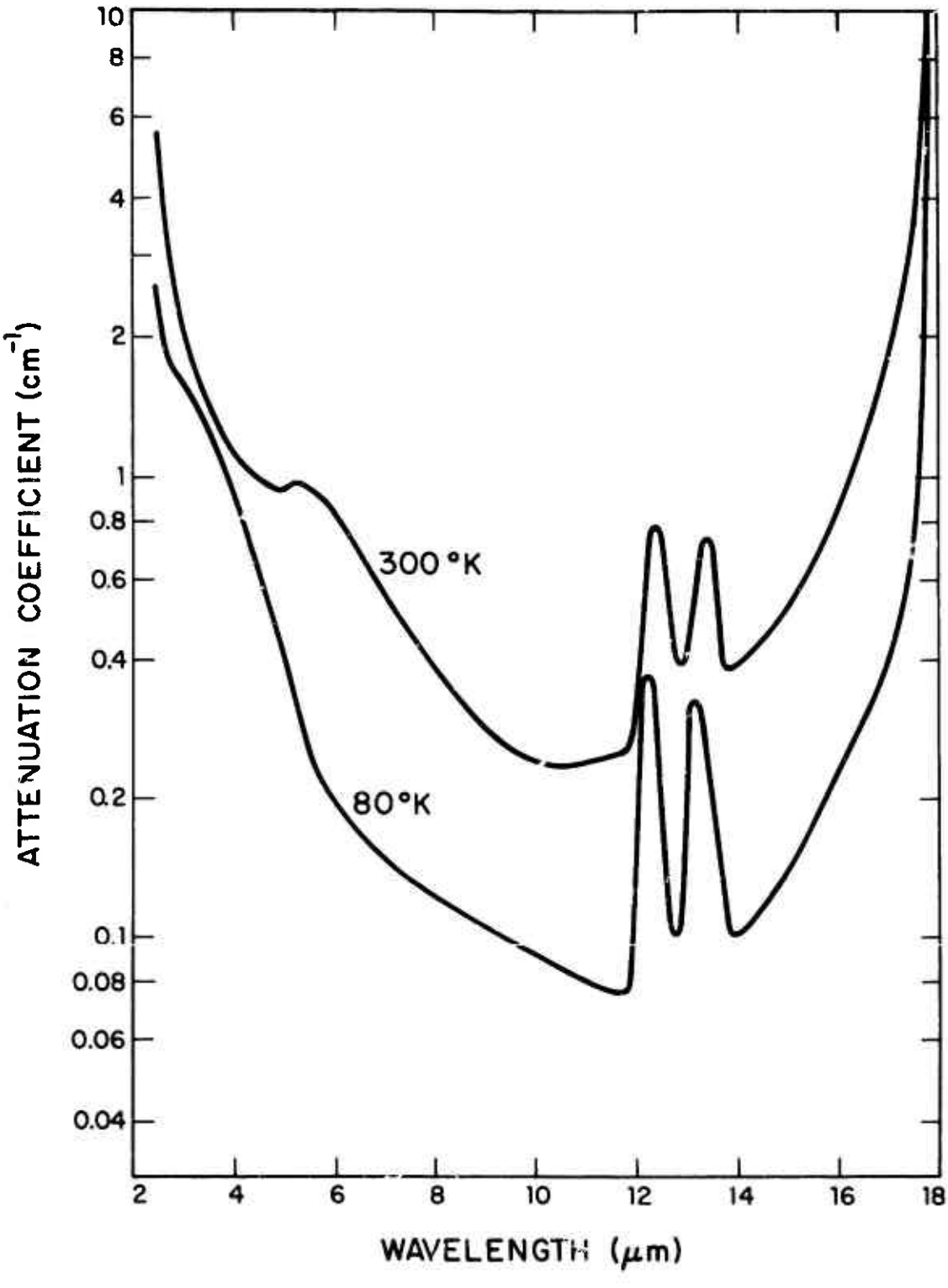

OPTICAL ATTENUATION OF $CdGeAs_2$

Fig. 1.1-2

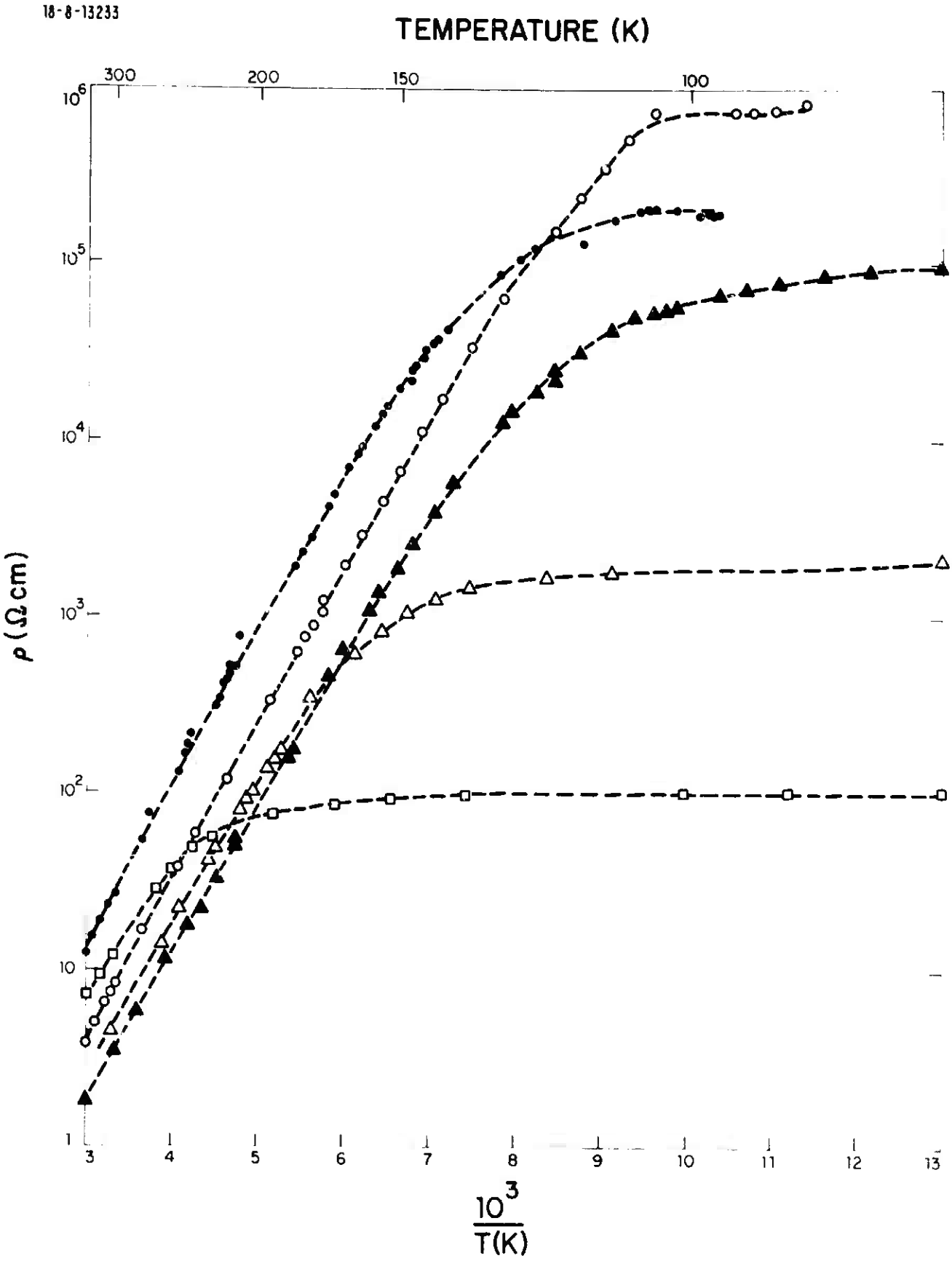
18-8-13233
TEMPERATURE (K)
300
200
150
100
10^6
10^5
10^4
10^3
10^2
10
1
ρ (Ω cm)
3
4
5
6
7
8
9
10
11
12
13
$\frac{10^3}{T(K)}$

Fig. 1.1-3

18-8-13234

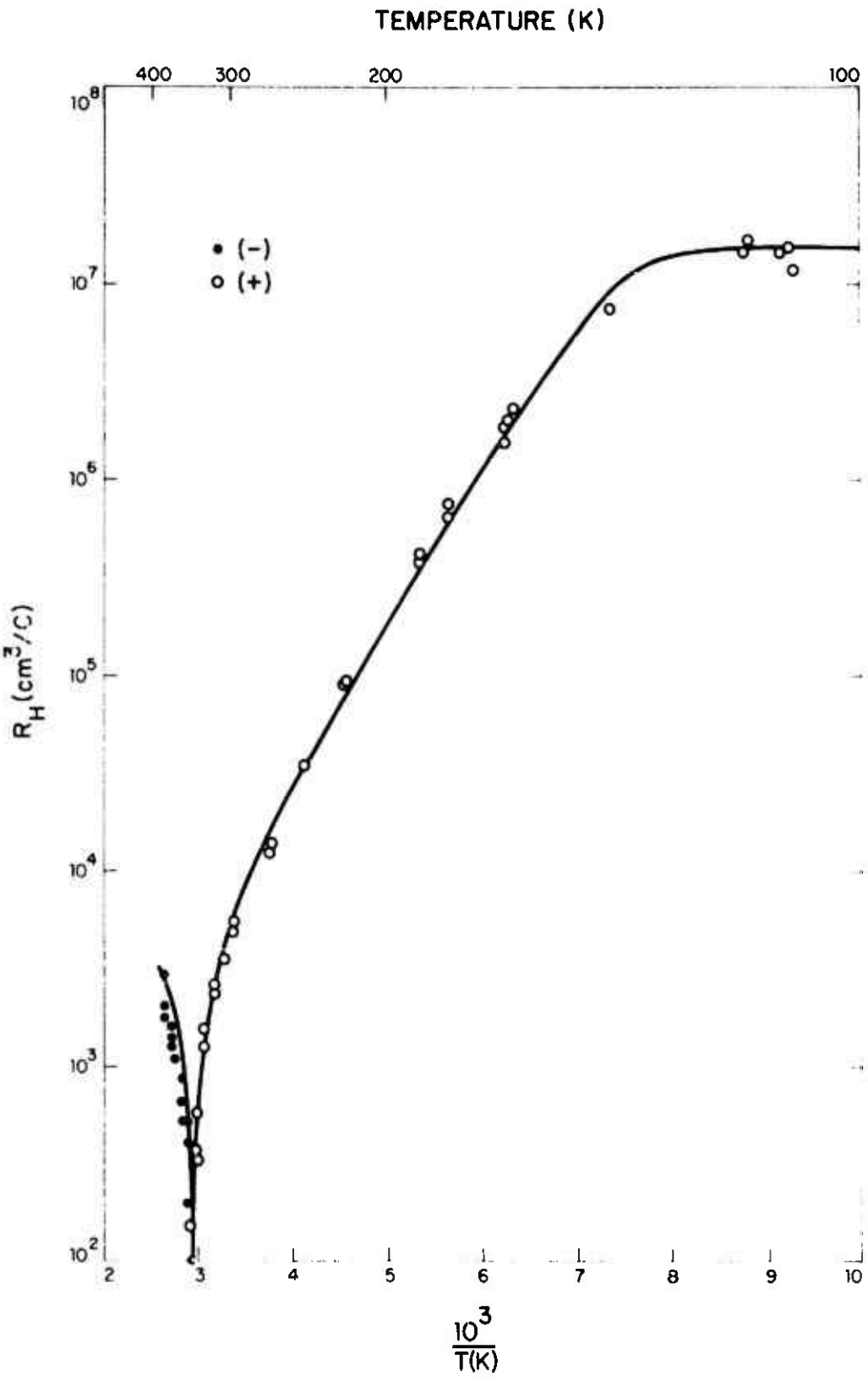

Fig. 1.1-4

1.2 $AgGaSe_2$

We have obtained two single crystal ingots of $AgGaSe_2$ by seeding two consecutive Bridgman growths in high temperature gradients. Seeds about 6 mm square by 30-35 mm long were cut with their c axes parallel to their long dimensions. One of them was inserted into a square tube section at the bottom of a quartz growth ampoule, which widened out from the 6 mm square at the seed to a 25 mm diameter at the top. About 170 grams of prereacted material was then loaded into the ampoule. A thermocouple junction was tied to the outside of the square tube at the center of the seed and the sealed ampoule was raised into the upper hot zone of a growth furnace until the thermocouple indicated 850°C. The ampoule was then lowered at a growth rate of 1 cm per day. Neither ampoule broke during cooling and both ingots slid out easily. Laue x-ray patterns showed that each ingot is a single crystal and that each has the same orientation as that of the seed; the c axis parallel to the cylindrical axis of the ampoule. Figure 1.2-1 is a picture of one of the ingots which was grown from a melt of composition $AgGaSe_{2.005}$. This crystal contains some precipitates which scatter light and reduce the transmission of a 6.3 mm sample 18% below the reflectivity limit at 2.5 μm. The other ingot was grown from a melt with composition $AgGaSe_{2.01}$ and it contains less precipitates but some cracks. Each ingot has less precipitates near the outside edges than at the center due to the more rapid cooling at the outside and therefore spend less time at the temperatures where precipitation occurs.

On the basis of our results we believe that seeded Bridgman growth is a practical way to avoid the cracking which otherwise takes place because of the negative thermal expansion[1.1-4] parallel to the c axis. Our earlier experiments as well as those of Matthes et al.[1.1-5] for $AgGaS_2$ have shown that it should be possible to grow

crystals of $AgGaSe_2$ essentially free of precipitates, by optimizing the amount of excess Se and Ag in the melt. Further work is in progress.

G. W. Iseler

References:

1.2-1 Quarterly Progress Report, Lincoln Laboratory, M.I.T., 1 July-30 September 1974 to LASL on the Program in Support of the JUMPer Program.

1.2-2 H. Matthes, R. Viehmann and N. Marschall, Appl. Phys. Lett. 26, 237 (1975).

Figure Caption:

1.2-1 $AgGaSe_2$ ingot grown by seeded Bridgman method.

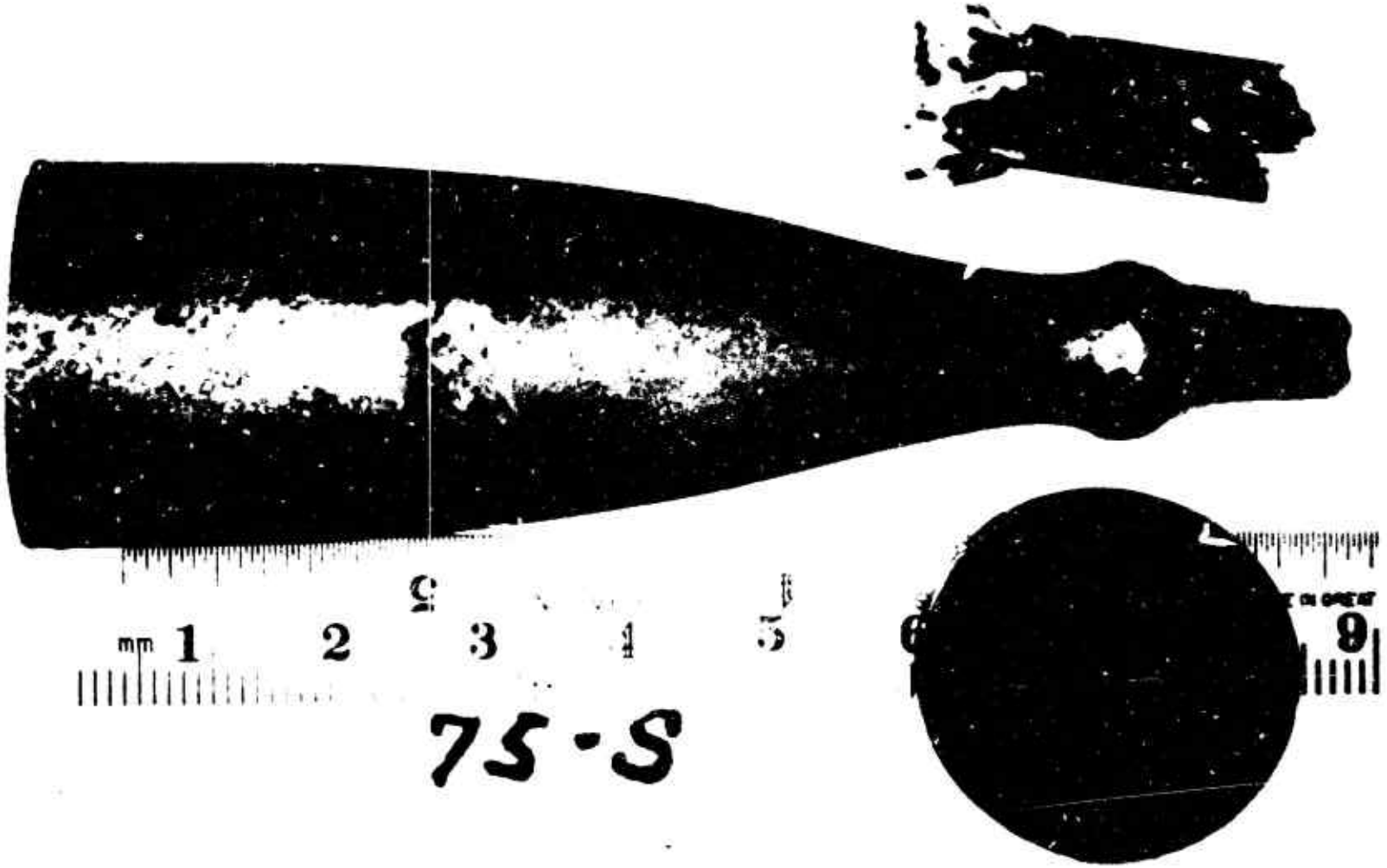

Fig. 1.2-1

2. APPLICATION OF INFRARED NONLINEAR MATERIALS

2.1 Efficient, High Average Power SHG in $CdGeAs_2$

The second harmonic generation (SHG) in $CdGeAs_2$ crystals subjected to intense focused CO_2 radiation is being studied. Conversion efficiency of the samples has been investigated for both cw and Q-switched operation of the pump laser. A tunable CO_2 laser with a 1.75 m spacing between the grating and the output coupler mirror was used in our experiments. The laser is capable of producing over 20 Watts cw when tuned to the P(20) transition of the $(00^0 1) - (10^0 0)$ band.

The same laser is used for the Q-switching experiments, but with a system of two lenses and a chopper wheel inserted between the CO_2 cavity window and the grating. The arrangement is shown in Fig. 2.1-1. The chopper wheel is located at the focal point of two AR coated ZnSe lenses with f = 3.5 cm. The wheels, which consist of equally spaced knife-edged slots, are attached to a high-speed motor capable of over 13,000 rpm. Average output powers over 10 W have been achieved at the highest rotation speeds using a 180-slot wheel, each 8 mils wide. Peak powers well over a kilowatt have been obtained with this system.

a) cw Second Harmonic Generation

The samples investigated to date were obtained from two boules (#74-32 and #76-5) which were found to have relatively low absorption at the doubled frequency. These samples, oriented for Class I phasematching, were placed in a liquid nitrogen Dewar to further reduce absorption. The samples varied in length from 4 to 13 mm, with varying cross-sectional areas, down to 1.5 x 3 mm. The radius of the focused beam waist, as determined by calibrated aperture measurements, was approximately 90 μm.

The second harmonic power generated in the initial experiments carried out using uncoated samples showed the expected $P(2\omega) \propto P(\omega)^2$ dependence, with no indication of saturation or thermal degradation even after increasing the effective pump level available by overcoming the large reflective losses at the

vacuum-$CdGeAs_2$ interfaces. This was done by evaporating a zinc sulfide coating on the front and rear surfaces of the samples to optimize transmission at wavelengths of 10.6 and 5.3 μm respectively. By this means the transmission at each face can be increased from 69% to 97%. The effect of anti-reflection coating upon second harmonic generation in sample #76-5N is shown in Fig. 2.1-2, where the second harmonic power emerging from a $CdGeAs_2$ sample is given as a function of the CO_2 power incident upon the front surface. The two curves were taken with the same sample, before and after AR coating. The two dashed lines are related by the ratio $(0.97/0.69)^3$. The figure shows no indication of saturation at the highest pump levels, which correspond to intensities of the order of 10^5 W/cm^2, and no signal degradation was observed while maintaining this level for several minutes.

While most samples investigated withstood the input levels discussed above, the damage threshold of one sample was reached at 3×10^4 W/cm^2 and in another at about 5×10^4 W/cm^2. The damage was manifested by a sudden and total disappearance of second harmonic, with no apparent signal degradation before the occurrence. After reaching the damage threshold, a fine ash deposit is observed on the Dewar window, and a hole $\sim$ 150 μm diameter and $\sim$ 1 mm depth is formed on the front face of the sample, with indications of surface melting. The back surface of the sample remains undamaged. These results are in marked contrast with the pit and plasma formation observed in $CdGeAs_2$ when subjected to high-energy pulsed input.[2.1-1] The cw damage appears to be consistent with the "thermal-runaway" mechanism which has been proposed to explain the damage in semiconductors used as high-power window materials.[2.1-2]

The thermal conductivity, K, of $CdGeAs_2$ is increasing rapidly with decreasing temperatures at the lowest temperatures measured ($K \propto T^{-1.7}$ at $T = 100^oK$).[2.1-3] Reducing the sample temperature should therefore result in a significant increase in the damage threshold.

b) Q-switched Second Harmonic Generation

For Q-switching, a slotted chopper wheel is located at the common focal point of two AR coated, f = 3.5 cm, ZnSe lenses, where the computed beam diameter is 83 μm.[2.1-4] Several wheels, with varying numbers of equidistant slots and slot widths have been used. The slots of the wheels with 180 and 90 slots are nominally 8 mils wide, while those on the 45- and 30-slot wheels are nominally 6 mils wide. It has been found that, in addition to slot width variation within each wheel (~ ± 5%), there are significant differences in the average width values of the two wheel pairs. This has made certain quantitative comparisons difficult, as will be discussed below.

A fast-switching laser should have the full beam width appear in the slot in a time period short compared to the pulse build-up time τ. For $\tau_B \sim 400$ ns, the wheel velocity $\underline{v}$ at the beam waist should be greater than 2.1×10^4 cm/sec. In our experimental arrangement, the velocity was limited to $v \cdot 7.3 \times 10^3$ cm/sec. However, we found no indication of the multiple pulses predicted for slow switching by Hellwarth[2.1-5] and observed by Meyerhofer.[2.1-6] Instead, after a rapid pulse rise and partial decay, with a FWHM of approximately 200 ns, the pulse reaches a low level which slowly decreases until the end of the pulse is reached. Reducing the chopper-wheel velocity results in a "stretching-out" of the low-level region. This is seen in Fig. 2.1-3, which shows the CO_2 laser pulse using the 180-slot chopper wheel rotating at velocities of 6.2×10^3 cm/sec (40 kHz pulse rate) and 3.1×10^3 cm/sec (20 kHz). The spread of lines at the end of the pulse is indicative of the variation of slot widths. The most notable effect of further velocity reduction down to ~ 500 cm/sec is a significant decrease in the initial pulse height.

The effect of varying the wheel velocity upon the average value of the CO_2 laser output and the second harmonic generated is shown in Fig. 2.1-4. Although the ratio of on/off time is independent of velocity, more of the output pulse occurs in the low-level region as the wheel slows down; hence the observed decrease of

average laser output with decreasing velocity. The second harmonic output drops more rapidly than the CO_2 output, resulting in a decreasing SHG efficiency with decreasing velocity.

An alternative method of varying the pulse rate is to maintain a constant wheel velocity but changing the number of slots per wheel. The variation of the average second harmonic power generation as a function of the square of the Q-switched CO_2 laser input power is given in Fig. 2.1-5 for the four wheels previously described. The wheel velocity in all four cases was $v = 6.2 \times 10^3$ cm/sec. The experimental results shown in Fig. 2.1-5 were obtained using a premixed gas cylinder with a 1:3:18 ratio of CO_2:N_2:He, and the CO_2 laser power was varied by changing the electrical energy input and the gas pressure in the laser tube. Although the gas mixture was not optimum for achieving maximum laser power, the use of a premixed gas ensured similar laser conditions for all the curves.

The increase in the slope of the curves with decreasing pulse rate in Fig. 2.1-5 is expected in view of the results given in Appendix 2.1-A, where it is shown that for a fixed pulse shape the slope of the curves are inversely proportional to the pump frequency. However, the accord is only qualitative since the pulse shapes are different for the different wheels. This is true even for wheel pairs which are nominally of the same slot widths. The difference is due in part to width variations within each wheel, but primarily to the variation in the average width between wheel pairs of nominally equal slot widths; most notably between the 90- and 180-slot wheels. Finally, if the period between pulses is too short to permit the maximum inversion buildup, the peak power will vary with the number of wheel slots. Relative values of the CO_2 laser peak power as a function of pulse separation under fixed electrical input power conditions is shown in Fig. 2.1-6. Although the effect is decreasing, the peak power is still rising at the longest pulse separation times measured. Hence,

even if the slot widths were the same, there would still be some variation from the inverse frequency relationship derived in Appendix 2.1-A.

As noted previously, the premixed gas ratio used in obtaining the results of Fig. 2.1-5 was not suitable for maximizing the laser output power under Q-switching conditions. The maximum average CO_2 laser input to the $CdGeAs_2$ sample achieved to date is 8.6 W, obtained with the 180-slot wheel at a 40 kHz pulse rate and a CO_2:N_2:He ratio of 1:1.4:4. The corresponding average SHG power emitted by our sample was 640 mW.

Although this is the highest average SHG power obtained, the overall power efficiency is 7.5%. This relatively low value is not surprising, since, as shown in Eq. (2) of Appendix 2.1-A, the efficiency is not proportional to the average CO_2 laser power, but rather to the effective power output per pulse. This should be lowest for the 180-slot wheel since 1) it has 8-mil slots, so the laser output is low for a significant portion of the pulse and 2) the peak power level, as given in Fig. 2.1-6, is lowest for this wheel.

Using the 30-slot wheel at a pulse rate of 7.8 kHz and a gas ratio of 1:1:3.2, a maximum external overall power efficiency of 18% was obtained ($<P_{\omega}>$ = 2.4 W; $<P_{2\omega}>$ = 0.43 W). This corresponds to an internal power efficiency of ~ 19%. The highest external efficiency previously reported was 12.8%,[2.1-1] obtained with a CO_2 TEA laser using an uncoated $CdGeAs_2$ sample at liquid nitrogen temperature. Corrected for reflection losses, that corresponds to an internal conversion efficiency of 27.6%. It should be noted that the use of a TEA laser severely restricts the pulse rate. The above measurement[2.1-1] was made at 1 pps.

Both the CO_2 laser input pulse and the corresponding second harmonic pulse for which 18% conversion efficiency was obtained are shown in Fig. 2.1-7. They indicate peak powers of approximately 1200 W and 325 W at 10.6 and 5.3 μm

respectively, corresponding to an external peak power efficiency of 27%. There is no indication of saturation at this conversion level.

The results of Fig. 2.1-6 indicate that higher peak power efficiencies will be obtainable using longer pulse intervals. To establish this, wheels with as few as 2 slots will be investigated. In addition, improved methods for generating narrow slots of well-defined width on the chopper wheel are being pursued.

N. Menyuk

APPENDIX 2.1-A

The instantaneous value of the second harmonic power generated is proportional to the square of the instantaneous CO_2 laser pump power. We can approximate this over a single pulse by the relationship $P_{2\omega}(\text{eff}) = K P_{\omega}^{2}(\text{eff})$, where $P_{2\omega}(\text{eff})$ and $P_{\omega}^{2}(\text{eff})$ are the effective pulse power levels $\frac{1}{\tau}\int_{0}^{\tau} P_{2\omega}\, dt$ and $\frac{1}{\tau}\int_{0}^{\tau} P_{\omega}^{2}\, dt$ respectively, where τ is the pulse length and K is a proportionality constant. The average second harmonic power $\langle P_{2\omega}\rangle$, as measured by a thermopile detector, is given by $\langle P_{2\omega}\rangle = \nu P_{2\omega}(\text{eff}) = K\nu P_{\omega}^{2}(\text{eff})$, where ν is the pulse frequency. Similarly, the average CO_2 pump laser output $\langle P_{\omega}\rangle = \nu P_{\omega}(\text{eff})$. For a given pulse shape, the ratio $P_{\omega}^{2}(\text{eff})/(P_{\omega}(\text{eff}))^{2} = \alpha$ is a constant. In that case the average second harmonic power is related to the average CO_2 pump power by

$$\langle P_{2\omega}\rangle = \frac{K'}{\nu}\langle P_{\omega}\rangle^{2} \tag{1}$$

and the average second harmonic generation efficiency

$$\frac{\langle P_{2\omega}\rangle}{\langle P_{\omega}\rangle} = K' P_{\omega}(\text{eff}) \quad , \tag{2}$$

where K' is a new proportionality constant equal to αK.

References:

2.1-1 Solid State Research Report, Lincoln Laboratory, M.I.T., (1975:2), p. 23.

2.1-2 F. A. Horrigan, C. A. Klein, R. J. Rudko and D. T. Wilson, "High Power Gas Laser Research," Final Technical Report on Contract No. DA-AH01-67-1589, Raytheon Research Division, September 1968, pp. 59-64.

2.1-3 P. Leroux-Hugon, Comptes Rendus 236, 3991 (1963).

2.1-4 H. Kogelnik and T. Li, Proc. IEEE, 54, 1312 (1966).

2.1-5 R. W. Hellwarth in Lasers, vol. 1, A. K. Levine, Editor, (M. Dekker, Inc., New York, 1966).

2.1-6 D. Meyerhofer, IEEE J. Quantum Electron. QE-4, 762 (1968).

Figure Captions:

2.1-1 Schematic arrangement of chopper-wheel Q-switched CO_2 laser.

2.1-2 Variation of cw second harmonic power output with CO_2 laser input power. Also shown is the effect of anti-reflection coating. The two dashed lines are related by the ratio $(0.97/0.69)^3$.

2.1-3 Effect of velocity change upon pulse shape of Q-switched CO_2 laser using 180-slot chopper wheel.

2.1-4 Effect of velocity change upon the CO_2 laser pump power and the corresponding second harmonic power using 180-slot chopper wheel.

2.1-5 Effect of varying wheel slot spacing upon second harmonic generation at constant velocity.

2.1-6 Relative laser pump peak power as a function of pulse separation.

2.1-7 CO_2 laser pump pulse and corresponding second harmonic pulse. Energy per pulse: 10.6 μm, 307 μJ; 5.3 μm, 55 μJ. Pulse rate: 7.8 kHz.

18-8-13229

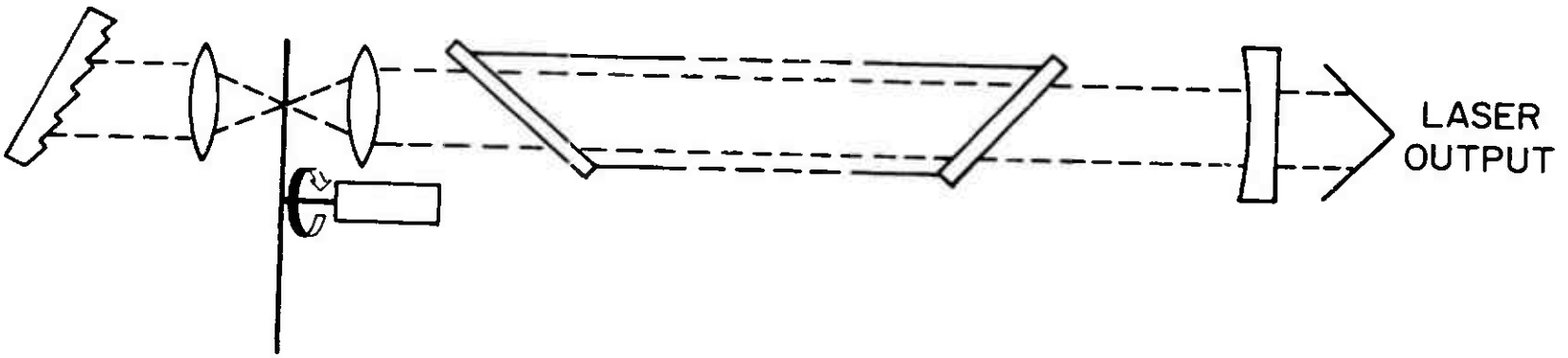

Fig. 2.1-1

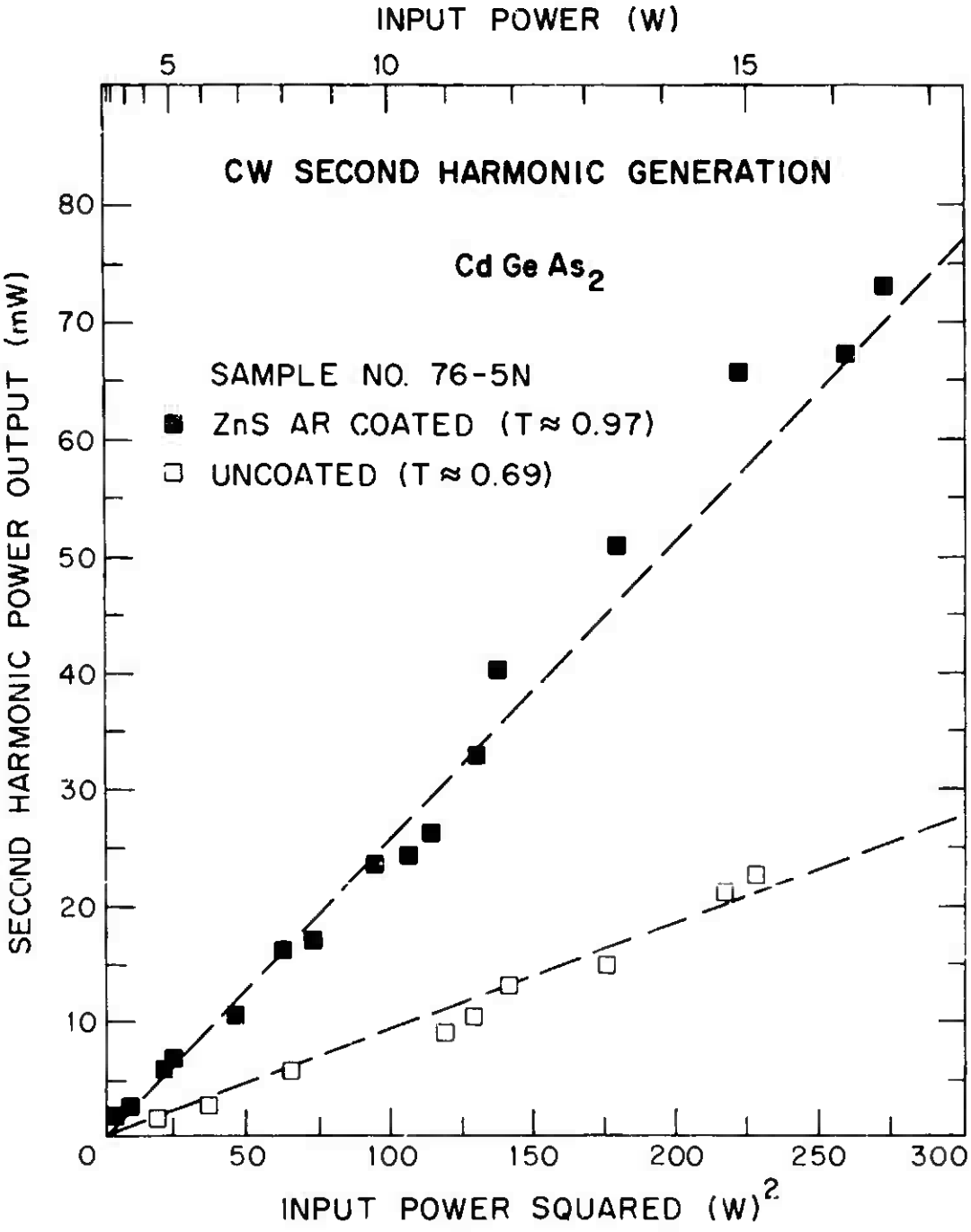
INPUT POWER (W)
5
10
15
CW SECOND HARMONIC GENERATION
Cd Ge As2
SAMPLE NO. 76-5N
ZnS AR COATED (T≈0.97)
UNCOATED (T≈0.69)
SECOND HARMONIC POWER OUTPUT (mW)
0
10
20
30
40
50
60
70
80
0
50
100
150
200
250
300
INPUT POWER SQUARED (W)2

Fig. 2.1-2

VELOCITY
(pulse rate)

3.1×10^3 cm/sec
(20 kHz)

6.2×10^3 cm/sec
(40 kHz)

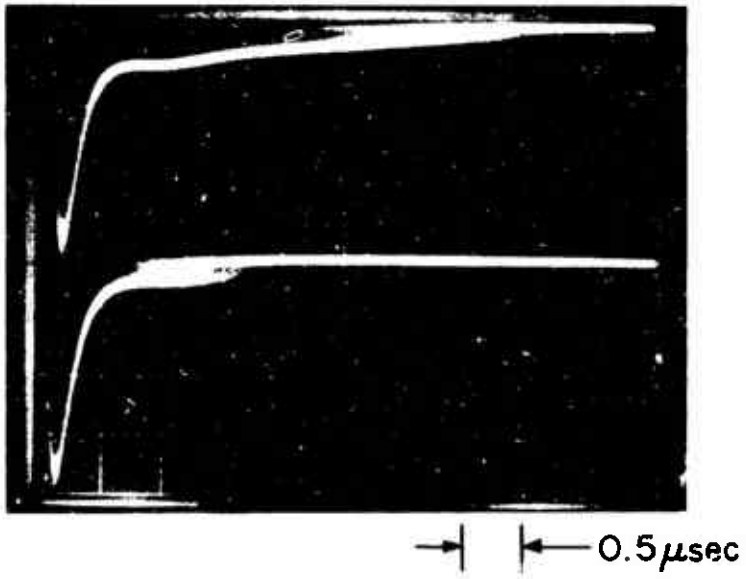

Fig. 2.1-3

18-8-13231

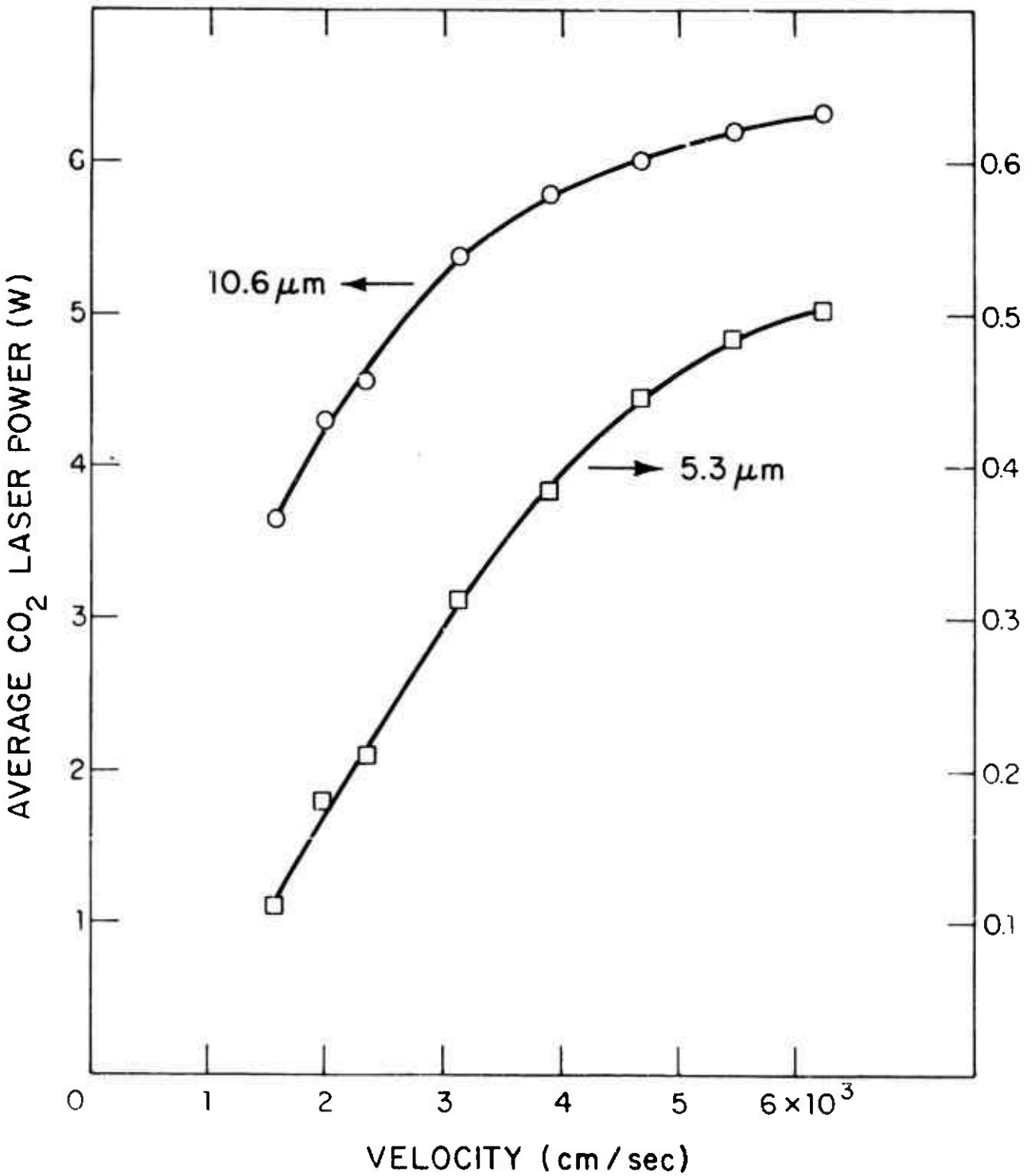

Fig. 2.1-

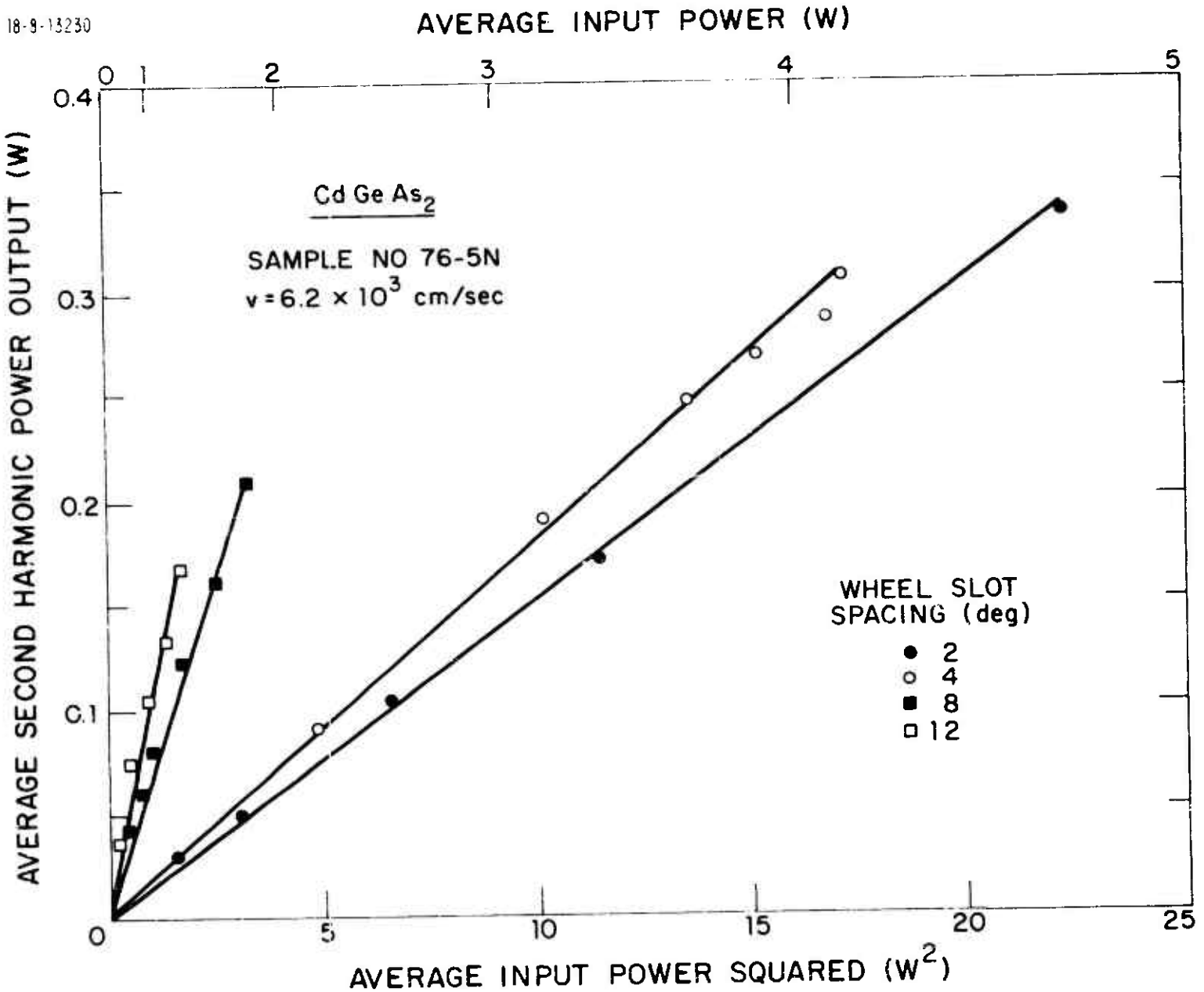
18-9-13230
AVERAGE INPUT POWER (W)
0
1
2
3
4
5
0.4
0.3
0.2
0.1
0
AVERAGE SECOND HARMONIC POWER OUTPUT (W)
Cd Ge As2
SAMPLE NO 76-5N
v = 6.2 × 10^3 cm/sec
WHEEL SLOT SPACING (deg)
2
4
8
12
5
10
15
20
25
AVERAGE INPUT POWER SQUARED (W^2)

Fig. 2.1-5

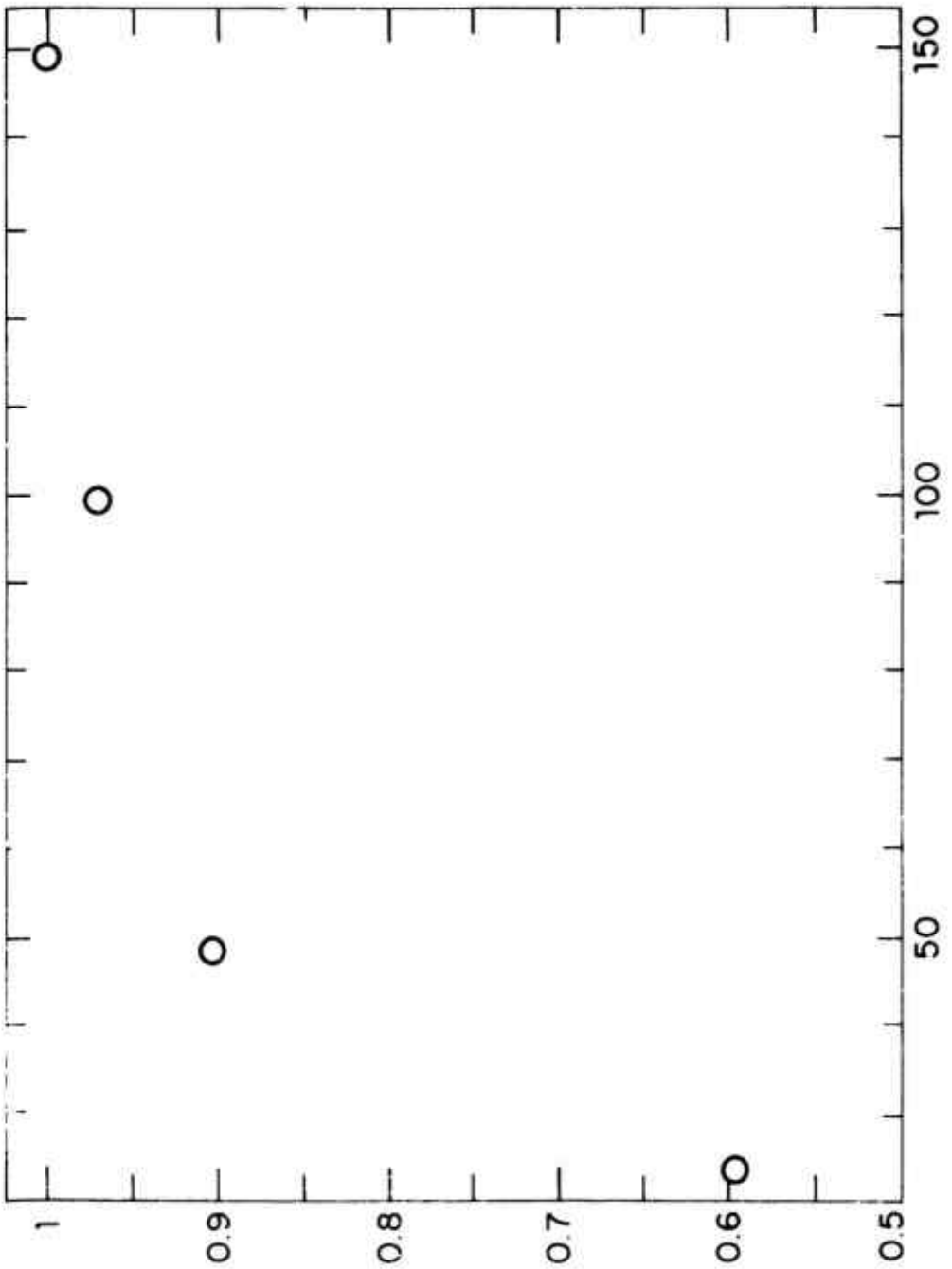

18-8-13228

Fig. 2.1-6

SECOND HARMONIC
AT 5.3 μm

CO_2 LASER PUMP
AT 10.6μm

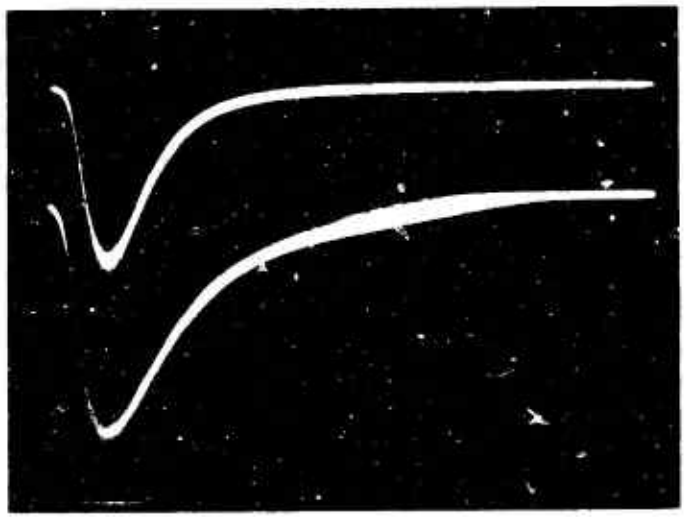

0.1μsec

Fig. 2.1-7

2.2 Average Second Harmonic Power Limitations in $CdGeAs_2$

The high peak power pulsed second harmonic generation (SHG) experiments using $CdGeAs_2$ crystals performed to date have used low repetition rates of approximately 1 Hz; recently we have investigated the performance of these crystals at higher repetition rates using a CO_2 TEA laser in order to investigate the average power handling capability of the crystals. Other experiments, performed by N. Menyuk have used a Q-switched CO_2 laser capable of still higher repetition rates but with lower energy per pulse.

The CO_2 TEA laser used in these experiments was capable of producing 0.7 J pulses at rates up to 25 Hz and 0.34 J pulses at rates of up to 50 Hz. The multimode, single line (P(24) of the 9.6 μm band), output was passed through a beam reducing telescope which produced a spot size of 3.3 mm. The doubling crystal, 74-36-C, had a cross section of 11 x 13 mm and a length of 10 mm. This crystal which has higher absorption losses than our best doubling crystals was used because of its large aperture. The crystal was mounted in a liquid nitrogen Dewar by different techniques, described below. The laser energy, as well as the SH energy, was measured using a Gen-Tec pyroelectric joulemeter; the average SH power was measured with a Scientech meter.

The maximum SH energy per pulse was limited by the available laser energy; no visible glow indicating optical damage was seen. Examination of the SH pulse shape showed a width of 130 nsec, FWHM. The CO_2 TEA laser gas mix was adjusted to be lean in nitrogen, in order to minimize the nitrogen tail on the pulse and increase the peak power. The maximum output energy per pulse was 21 mJ at a rate of 4 Hz, measured at the exit window of the Dewar, for an input energy of 0.7 J incident on the entrance window.

In the initial experiments the crystal was contacted to the Dewar tail section by only one surface and was held in position by spring loading. At the maximum

laser energy of 0.7 J and repetition rates of 10 Hz, the SH power dropped within a few seconds, but returned to the original value if the beam was blocked for about a minute. Measurements of SH power versus pulse repetition frequency, shown in Fig. 2.2-1, deviated from a straight line at the higher rates. Both these results suggested the sample was being heated by the beam to the point where thermal runaway occurs. A number of different heat sinking techniques were tried, the most successful being one in which the crystal was placed into a close fitting "U" shaped copper yoke, contact to the sides being made by a mixture of Cry-Con grease and Apiezon N. The yoke was closed by another piece of copper, with indium foil being used to make good thermal contact. Figure 2.2-2 shows the SH power versus p.r.f. curve for this case. The SH power output of 0.22 W at 20 Hz could now be maintained for ~ 1 minute, the limit being imposed by the tendency of the TEA laser to arc at these repetition rates.

The TEA laser could be operated at repetition rates greater than 20 Hz by halving the size of the energy storage capacitor to 0.03 μFd; the output energy was then ~ 0.34 J/pulse. Under these conditions, average second harmonic powers of 0.31 W were obtained at 50 Hz using the improved heat sink described. The SH power dropped within a minute or so, suggesting heating was again occurring.

A technique for indium soldering $CdGeAs_2$ to copper blocks was developed. These samples did not crack with repeated thermal cycling. The soldering technique will be used to mount samples in the Dewar in future experiments.

The temperature rise at the center of the rectangular $CdGeAs_2$ crystal can be estimated using an expression derived for an edge cooled circular window of radius R, with the temperature of the edge pinned to T_o. The temperature T(0) at the center of the window is found to be

$$T(0) = T_o + \frac{\beta P}{4\pi K}(1 + 2 \ln R/\rho_o) \quad .$$

Here ρ_0 is the Gaussian radius of the beam, β the absorption coefficient and K the thermal conductivity.[2.2-1] If the beam size is about the same size as the sample we can set $\rho_0 = R$ and obtain,

$$\Delta T = \frac{\beta P}{4\pi K} \quad ,$$

where ΔT is the temperature rise between the center and the edge of the window. It is important to remember that the optical absorption increases and the thermal conductivity decreases with increasing temperature, leading to thermal runaway above a critical power. By using the 77°K values[2.2-2] $\beta = 0.06\ cm^{-1}$ and $K = 0.25\ W/cm\text{-}^{o}K$ together with P = 15 W we obtain $\Delta T = 0.3^{o}C$. This temperature rise is too small to lead to thermal runaway and does not account for the observed behavior. A possible explanation may lie in the existence of small inclusions with higher absorption than the measured average absorption. Such inclusions could give rise to locally high temperatures; this heating could then raise the temperature of the surrounding material sufficiently to cause runaway. Inclusions of this kind would not be detected on the scans of 10 μm transmission and SHG routinely performed on each sample as long as they were uniformly distributed throughout the volume; this sample did in fact look uniform on these scans.

Further work to determine the cause of the apparent heating and to evaluate the performance of AR coated crystals is planned.

T. F. Deutsch
H. Kildal

References:

2.2-1 F. Horrigan and R. Rudko "Materials for High-Power CO_2 Lasers", Final Technical Report under Contract DAAH01-69-C-0038, Raytheon Research Division, Waltham, Massachusetts Internal #S-1176 (September, 1969).

2.2-2 P. Leroux-Hugon, Comptes Rendus 256, 3991 (1963).

Figure Caption:

2.2-1 Second harmonic power versus pulse repetition frequency for $CdGeAs_2$ at $77^{o}K$ (nominal) using two heat sinking techniques.

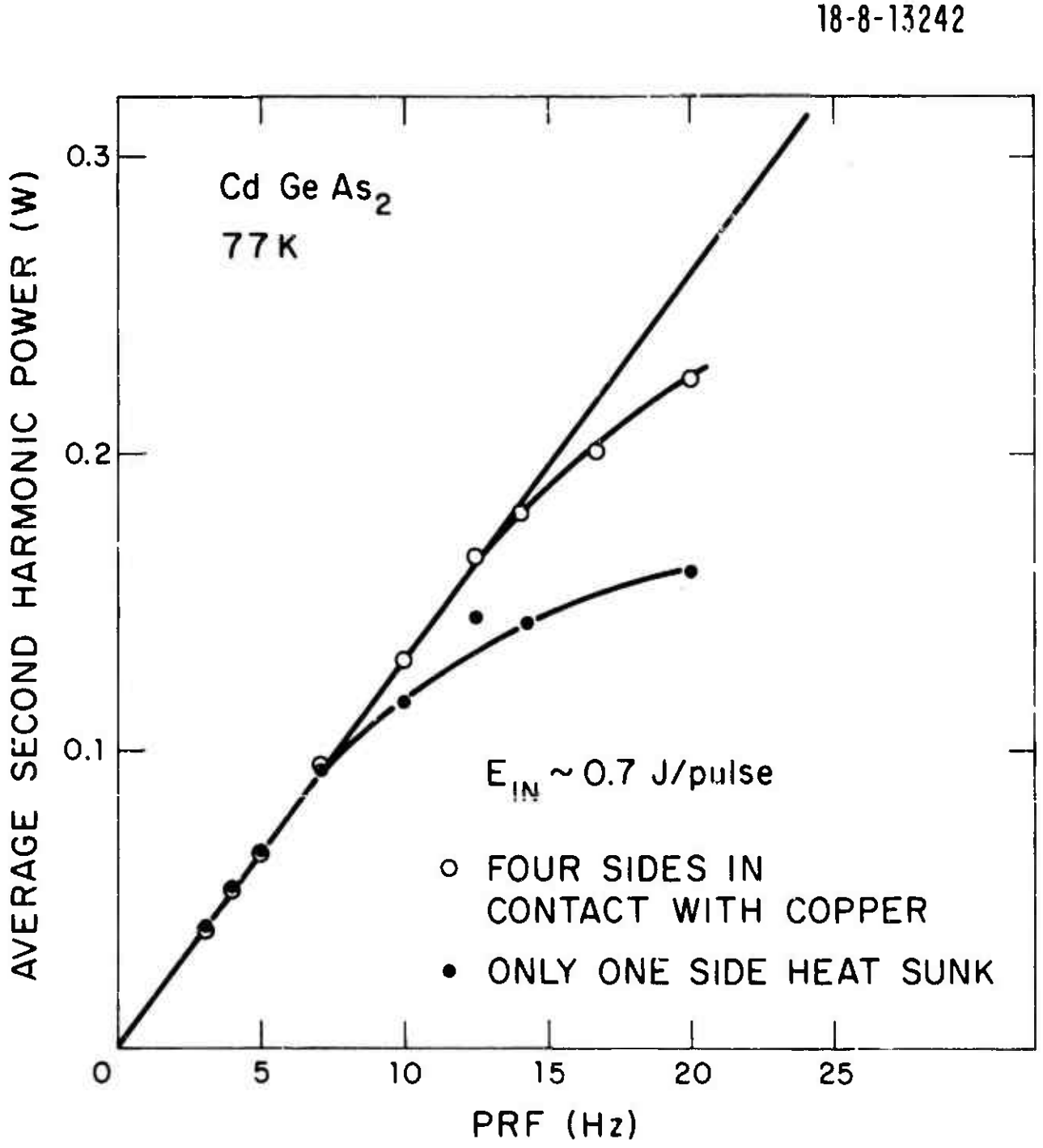
18-8-13242
Cd Ge As2
77 K
AVERAGE SECOND HARMONIC POWER (W)
0.3
0.2
0.1
0
5
10
15
20
25
PRF (Hz)
E_IN ~ 0.7 J/pulse
FOUR SIDES IN CONTACT WITH COPPER
ONLY ONE SIDE HEAT SUNK

Fig. 2.2-1

2.3 Difference Frequency Mixing in $CdGeAs_2$ at Liquid Nitrogen Temperature

The phasematching angles for difference frequency mixing in $CdGeAs_2$ at liquid nitrogen temperature has been measured for output wavelengths between 12.3 and 15.7 μm using a CO laser tuned between 5.39 and 5.96 μm and a CO_2 laser operated at 9.59 μm. Figure 2.3-1 shows the results together with the calculated phasematching curve using the indices of refraction data[2.3-1] and a previous room-temperature measurement on another sample.

As expected, there are only small changes in the phasematching angles between liquid nitrogen and room-temperature and it is not necessary to remeasure the indices of refraction at liquid nitrogen temperature to predict tuning curves for cooled $CdGeAs_2$ samples. The main difference in absolute measured angles for the two samples in Fig. 2.3-1 is due to the uncertainty in the crystal orientation ($\pm 0.5^{o}$) and the fact that there is a small variation in phasematching angles from boule to boule.

H. Kildal
G. W. Iseler

Reference:

2.3-1 H. Kildal and J. C. Mikkelsen, Optics Commun. 10, 306 (1974).

Figure Caption:

2.3-1 Output wavelength for CO-CO_2 laser mixing vs calculated and measured phasematching angles for type I phasematching in two samples of $CdGeAs_2$ the first cooled to liquid nitrogen temperature and the second at room-temperature.

18-8-12247 (1)

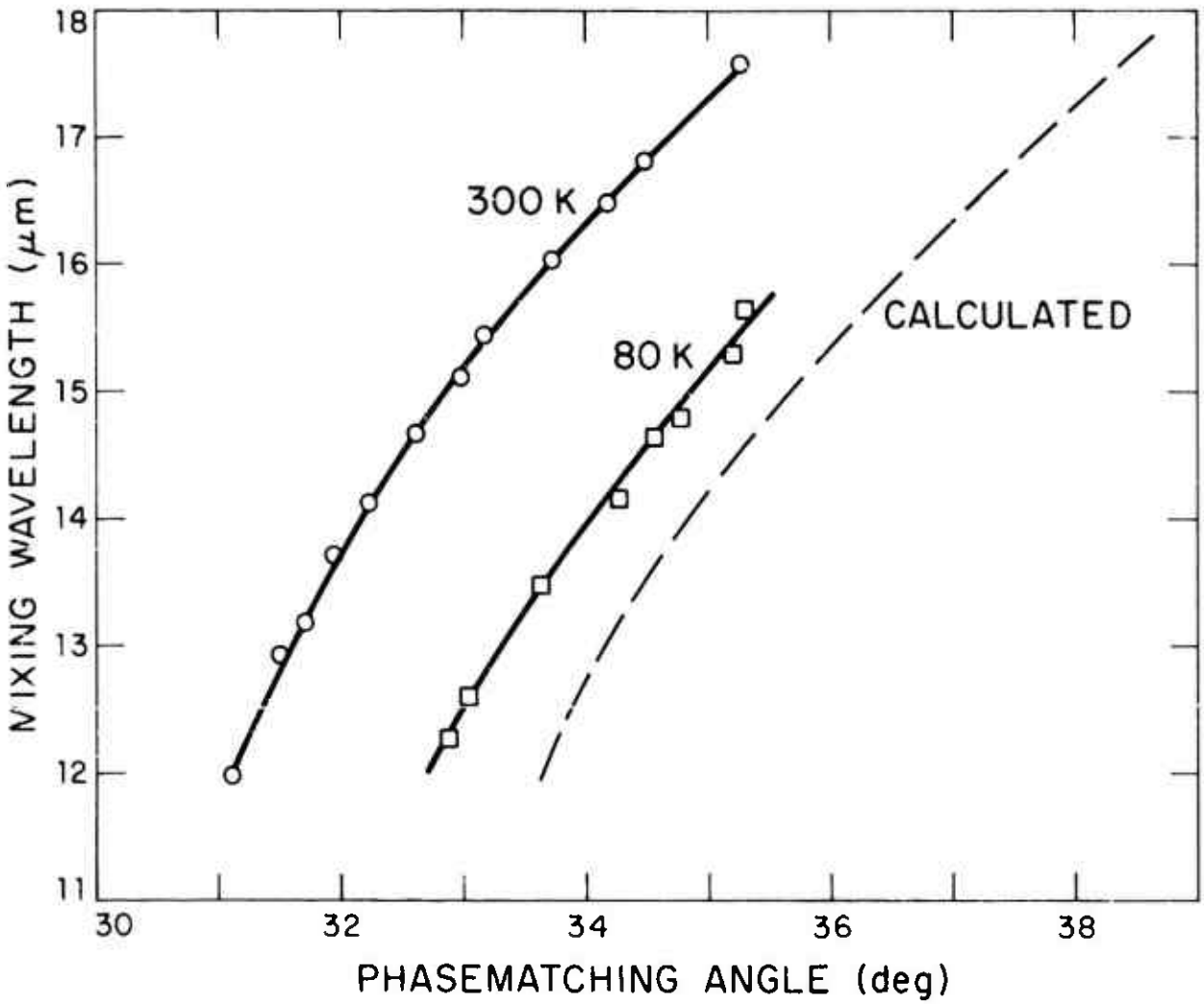

Fig. 2.3-1

3. OPTICALLY PUMPED TRANSFER LASERS

3.1 CO Transfer Lasers

a. New laser systems

i) SiH_4-CO

We have obtained laser action in SiH_4-CO mixes at pressures up to 35 Torr. This is the first reported laser action in SiH_4 and it is also the first time an optieally pumped energy transfer laser has been demonstrated for other than a linear moleeule. The thresholds for laser aetion in nonlinear moleeules are generally expected to be higher than for linear moleeules for several reasons. The rotational degeneracies are lifted, redueing the gain of eaeh vibrational-rotational transition. The number of modes of vibration is also larger, inereasing the number of ehannels for vihrational relaxation and making the production of an inversion more diffieult. The limitations due to rotational and vibrational relaxation can be overcome by using direet rather than transfer pumping and operating at suh-Torr pressures where no collisions occur during the pump pulse. This approaeh has been used to produee optically pumped laser aetion in SF_6[3.1-1]; however it requires an exact frequency match between the pump laser and the lasing moleeule.

A total of 6 SiH_4 laser lines has been observed in the 7.90 to 7.99 μm region. Table 3.1-1 lists the observed lines and Table 3.1-2 gives the four modes of the tetrahedral SiH_4 molecule. Only the ν_3 and the ν_4 modes are infrared aetive. The CO transfers energy into the ν_1 and the ν_3 modes. There are several possible laser transitions in the 8 μm region originating from these levels: $\nu_1 \rightarrow \nu_4$ (1272.8 cm^{-1}), $\nu_3 \rightarrow \nu_4$ (1276.4 cm^{-1}), and $\nu_3 \rightarrow \nu_2$ (1216.0 cm^{-1}). The speetroseopie eonstants for SiH_4 are not well enough known to identify the ohserved laser lines. We can only state that the lasing is not on the $\nu_3 \rightarrow \nu_2$ transition hecause its band eenter is too far away from the observed laser frequeneies.

The wavelength measurements were performed without any frequency seleeting element in the laser eavity. We tried to operate the laser with a grating in order to

extend the tuning range in the 7.9 μm region and to obtain laser action near 8.2 μm on the $\nu_3 \rightarrow \nu_2$ transition. The insertion losses, however, were too high to allow laser operation.

The optimum CO-SiH_4 mixing ratio was 1:1, although ratios from 1:3 to 4:1 were operated. Addition of helium was also tried, but did not increase either the output energy or the operating pressure; this is in contrast to its effect on the C_2H_2 and the CS_2 systems. Figure 3.1-1 shows the output energy versus input energy for a 1:1 mixture. The threshold is 1.7 mJ of pump energy delivered to the cell, and the slope efficiency is 0.5 percent with a maximum output energy of 0.03 mJ. The gain of the SiH_4-CO laser decreases linearly with pressure and the measured threshold of approximately 1/3 of the available pump energy at 12 Torr agrees well with the observed high pressure limit of 35 Torr.

Some minor problems were encountered because of the reactivity of the silane; a chemical reaction with the glass cell used initially caused some white deposits on the mirrors. The use of a brass cell, however, eliminated the problem.

ii) Other systems

We have also tried unsuccessfully to achieve laser action by energy transfer from CO to the tetrahedral molecules GeH_4 and CD_4. Table 3.1-2 lists the mode frequencies; the GeH_4-CO system, with band centers of respectively 1290.5 cm^{-1}, 1289.6 cm^{-1}, and 1180.9 cm^{-1} for the potential laser transitions $\nu_3 \rightarrow \nu_4$, $\nu_1 \rightarrow \nu_4$, and $\nu_3 \rightarrow \nu_2$, is of particular interest. The output mirror had a reflectivity of 98% at 1290 cm^{-1} (7.75 μm) and at 1250 cm^{-1} (7.94 μm^{-1}). The laser cell was aligned by optimizing the SiH_4 laser. The available pump energy was 6 times the SiH_4 threshold at 10 Torr. From the failure to obtain laser action in GeH_4 it follows that the gain is less than 1/6 of the gain in SiH_4. This is surprising. Spectroscopically the molecules are quite analogous and we therefore expected the CO energy transfer times and the self-deactivation rates to be very similar. Either this is not true or the SiH_4 has an anomalously high gain due to accidental line overlaps of different transitions. The fact

that six lines were observed makes the latter explanation unlikely. It was less surprising that the CD_4 did not lase. In this molecule the $2\nu_2$ and the $2\nu_4$ modes are in close resonance with the ν_1 mode thereby providing a pathway for rapid nearly resonant V-V deactivation of the ν_1 mode.

We have also tried unsuccessfully to obtain laser action in HCN by CO transfer into the ν_1 mode at 2089 cm^{-1} with possible laser action on the $\nu_1 \rightarrow \nu_2$ transition (1377 cm^{-1}). The gain on this transition is unknown although it is expected to be lower than on the $\nu_3 \rightarrow \nu_1$ transition (1223 cm^{-1}) which may be pumped using an HF laser to excite HF followed by energy transfer into the HCN ν_3 mode.

Another interesting system that we have investigated is the CH_3F-CO_2 system. The CH_3F was excited by the CO_2 P(20) line of the 9.6 μm band with the hope of obtaining energy transfer into the CO_2 $(10^00\text{-}02^00)_I$ or $(10^00\text{-}02^00)_{II}$ mode followed by laser action to the (010) level. This system is speculative since most of the important relaxation rates are unknown. The pay-off is obvious, however, if a 16 μm laser can be constructed with a CO_2 pump laser. The experiment was attempted in a 68 cm cell with dielectric mirrors and cooled to -80°C to reduce the population in the CO_2 (01^10) level. The output coupler had a reflectivity of 99 percent at 16 μm. The front mirror limited the input energy to the cell to 150 mJ because of optical damage problems. Laser action was not observed in this configuration.

h. High pressure operation and wavelength measurements for the C_2H_2-CO-He and the OCS-CO-He systems

We have investigated the upper pressure limit for laser action in C_2H_2 and OCS. The pressure limit is set by the deactivation rate of the upper laser level. Experimentally, it is found that the pump power necessary to reach threshold increases linearly with pressure until a certain pressure is reached above which the threshold suddenly starts to increase exponentially. This change in pressure dependence occurs when the deactivation time is comparable to the laser pulse length. Since the deactivation rate due to helium is usually slower than the self-deactivation rate, helium was added to the laser medium to

increase the pressure limits. The results for both gases are presented in Table 3.1-3.

In the acetylene laser experiments we used commercial C_2H_2 from which the standard traces of acetone were removed by a cold trap at -80°C. Figure 3.1-2, shows optical transmission of a cell filled with C_2H_2 with and without a cold trap. The C_2H_2 absorption around 7.5 μm is due to the combination band transition $\nu_4^1 + \nu_5^1$. The 8 μm C_2H_2 laser will also operate without removal of the acetone, but at a higher threshold.

Adding either He or H_2 to the C_2H_2-CO system improved the laser performance significantly. Besides raising the high pressure limit, it increased the maximum output power and the slope efficiency. In a 14 cm cell a maximum output power of 0.12 mj was obtained at 30 Torr with a C_2H_2-CO-H_2 ratio of 1:3:3. The maximum slope efficiency of 3.1% was observed in a C_2H_2-CO-He mixture of 1:3:30 at 250 Torr total pressure.

The encouraging high pressure results for C_2H_2 motivated us to attempt to run this gas in a UV preionized TEA laser configuration which should allow higher output energies. A cold trap was used to remove the acetone from the C_2H_2 before it was injected into the TEA laser cavity. CO-C_2H_2-H_2 and CO-C_2H_2-He laser mixes similar to those used in the optical pumping experiment were tried. We also attempted to obtain lasing by adding nitrogen to the discharge. However, no laser action was observed.

In the last semiannual progress report we reported the wavelength measurements for the C_2H_2 laser. We have now identified the laser emission as the Q(9), Q(11), Q(13), and Q(15) lines of the $01^100\text{-}00001^1$ transition. The observed lines, together with the measurements by Shelton and Byrne,[3.1-2] are listed in Table 3.1-4 and there is good agreement with the calculated frequencies. Only odd J transitions are observed since the odd rotational levels have three times the statistical weight of the even levels. We list also the Q-branch transitions for the C_2HD and the C_2D_2

molecules. These occur at respectively 1173 cm^{-1} (8.51 μm) and 1225 cm^{-1} (8.16 μm). It might be possible to extend the laser action in C_2H_2 to the P-branch by inserting a grating in the cavity. The R-branch is less likely because of the combination band absorption.

c. High pressure tunable CO_2 laser*

High pressure operation of optically pumped molecular lasers has the potential of continuous tunability. CO_2 is particularly suitable for high pressure operation because of its low self-deactivation rate of the 00^01 mode, 350 sec^{-1} $Torr^{-1}$. We have examined the high pressure operation of the CO_2-CO-He system. The use of helium rather than CO_2 for pressure broadening has certain advantages, since it pressure broadens CO_2 about 2/3 as much as CO_2 itself, but deactivates the CO_2 upper level only 1/4 as rapidly. The three component gas system thus allows the absorption of the pump laser, the density of the active medium, and the pressure broadening to be controlled somewhat independently.

We have operated the CO_2-CO-He system up to 16 atm, the limit imposed by the cell windows. For a 9:1:57 mixture in a 4.3 cm cell the measured threshold energy at 16 atm was 2.1 mJ, the slope efficiency was 6 percent, and the maximum output power was 0.25 mJ. The threshold did not change significantly between 10 and 16 atm. This is because the pressure broadening of the lines is now partially compensated by line overlap; at 16 atm the rotational lines of CO_2 are sufficiently broadened to allow continuous tuning. In addition because the CO lines are also broadened it is not necessary to rely on a specific coincidence between the CO_2 second harmonic and a CO absorption line. This was verified by producing laser action using the CO_2 P(20) and P(22) lines in the 9.6 μm band as well as the regular P(24) line.

In order to be useful as tunable sources, the high pressure CO_2 laser will need to incorporate a grating, an etalon, and apertures for mode selection in an

*This work was sponsored by the Department of the Air Force, and reported for information purposes.

external mirror cavity. The additional window losses and the increased build-up times in this configuration raised the 16 atm threshold to ~ 11 mJ in an external mirror cavity; grating tunable operation is estimated to require at least twice this energy and should be possible with the expected improvements in doubling technology. Such advances in second harmonic generation should make possible a high repetition rate, continuously tunable CO_2 laser.

d. Development of grating tuned $O^{12}CS$ and $O^{13}CS$ lasers

Some of the frequencies that would be generated by an $O^{13}CS$ laser may be useful for isotope separation. We have compared the performance of the two CO-OCS systems using $O^{13}CS$ supplied by LASL.

Tuning techniques were first examined using $O^{12}CS$ and a grating tuned OCS laser providing over 80 lines between 8.19 and 8.46 μm was developed. The $O^{12}CS$ laser output on the $00^{0}1$-$10^{0}0$ transition was tuned from R(8) to R(47) and from P(6) to P(48). Figure 3.1-3 shows the $O^{12}CS$ output energy versus input energy for different cavity combinations. In these measurements the second harmonic energy was focused by a 7.5" f.1 lens into the cavity. The threshold energy for a cavity with a Brewster window and a grating is 2.2 mJ, about ten times higher than for the internal mirror cavity.

We then tried to operate the grating tuned laser using O^{13} CS. The threshold, however, was higher than for $O^{12}CS$. The laser was barely above threshold and it was too unstable for any frequency measurements. Figure 3.1-4 shows the output energy versus input energy for a cavity with one external mirror and no focusing. The $O^{13}CS$ threshold is about a factor of two higher, which is probably partly due to a slower energy transfer from CO into OCS because of a larger frequency mismatch (134 cm^{-1} compared to 81 cm^{-1}) and also due to a faster deactivation of the upper laser level because of a stronger resonance between the $00^{0}1$ mode and the $12^{0}0$ and $04^{0}0$ modes.

In order to improve the performance of the grating tuned $O^{13}CS$ laser, we have tried different cavity designs including a three-mirror cavity with a ZnSe window AR-coated on one side replacing the Brewster window. This structure should reduce the insertion losses of the grating. Experimentally, however, the threshold remained approximately the same. We have also tested a 55 cm cell at -80°C. The room-temperature threshold was higher for this laser as shown in Fig. 3.1-5. However, at -80°C the threshold decreased by a factor of 3.5 and it was comparable to the room-temperature results for the 14 cm cell.

In order to determine the lasing lines we performed some preliminary frequency measurements on the $O^{13}CS$ laser with an internal mirror cavity. The measured lines are listed in Table 3.1-5. The frequencies of the OCS $00^01 \rightarrow 10^00$ transitions are given by

$$\nu(m) = \nu_o + (B_{00^01} + B_{10^00})\, m + (B_{00^01} - B_{10^00})\, m^2$$

where $\nu_{R(J)} = \nu(J + 1)$ for the R-branch and $\nu_{P(J)} = \nu(-J)$ for the P-branch. The $O^{13}CS$ band center ν_o is not known to better than a few wavenumbers. Using our preliminary measurements, however, together with the rotational constants $B_{00^01} = 0.2010460\ cm^{-1}$ and $B_{10^00} = 0.2015708\ cm^{-1}$ (3.1-3) we can estimate the $O^{13}CS$ laser lines near 1160 cm^{-1}. We find lines at $1159.84 \pm 0.1\ cm^{-1}$ and $1160.23 \pm 0.1\ cm^{-1}$ which are either R(10) and R(11) transitions or R(11) and R(12).

In the near future we hope to increase the SHG output energy to at least 100 mJ. The $O^{13}CS$ laser should then operate easily with a grating.

H. Kildal
T. F. Deutsch

References:

3.1-1. H. R. Fetterman, H. R. Schlossberg, and W. E. Barch, Optics Commun. 15, 358 (1975).

3.1-2. C. F. Shelton and F. T. Byrne, Appl. Phys. Lett. 17, 439 (1970).

3.1-3. Y. Morino and T. Nakagawa, J. Mol. Spectrosc. 26, 496 (1968).

Figure Captions:

3.1-1 Output energy versus input energy for the SiH_4 laser with a SiH_4-CO ratio of 1:1.

3.1-2 Optical transmission through 50 Torr of C_2H_2 in a 10 cm cell with and without removal of the acetone traces by a cold trap at -80°C.

3.1-3 Output energy versus input energy for the OCS laser at 12 Torr total pressure and 14 cm active length. Front optics: 1 m 99% R at 8.2 μm. Rear optics: 30 cm 100% Reflector (a), ZnSe Brewster window and 30 cm 100% Reflector (b), ZnSe Brewster window and grating blazed at 8 μm (c).

3.1-4 Output energy versus input energy for two OCS isotope lasers at 12 Torr total pressure and 14 cm active length. Front optics: 1 m 99% R at 8.2 μm. Rear optics: ZnSe Brewster window and 2 m 100% Reflector.

3.1-5 Output energy versus input energy for the OCS laser at two different temperatures and a 55 cm internal mirror cell. Front optics: 1 m 99% R at 8.2 μm. Rear optics: 2 m 100% Reflector.

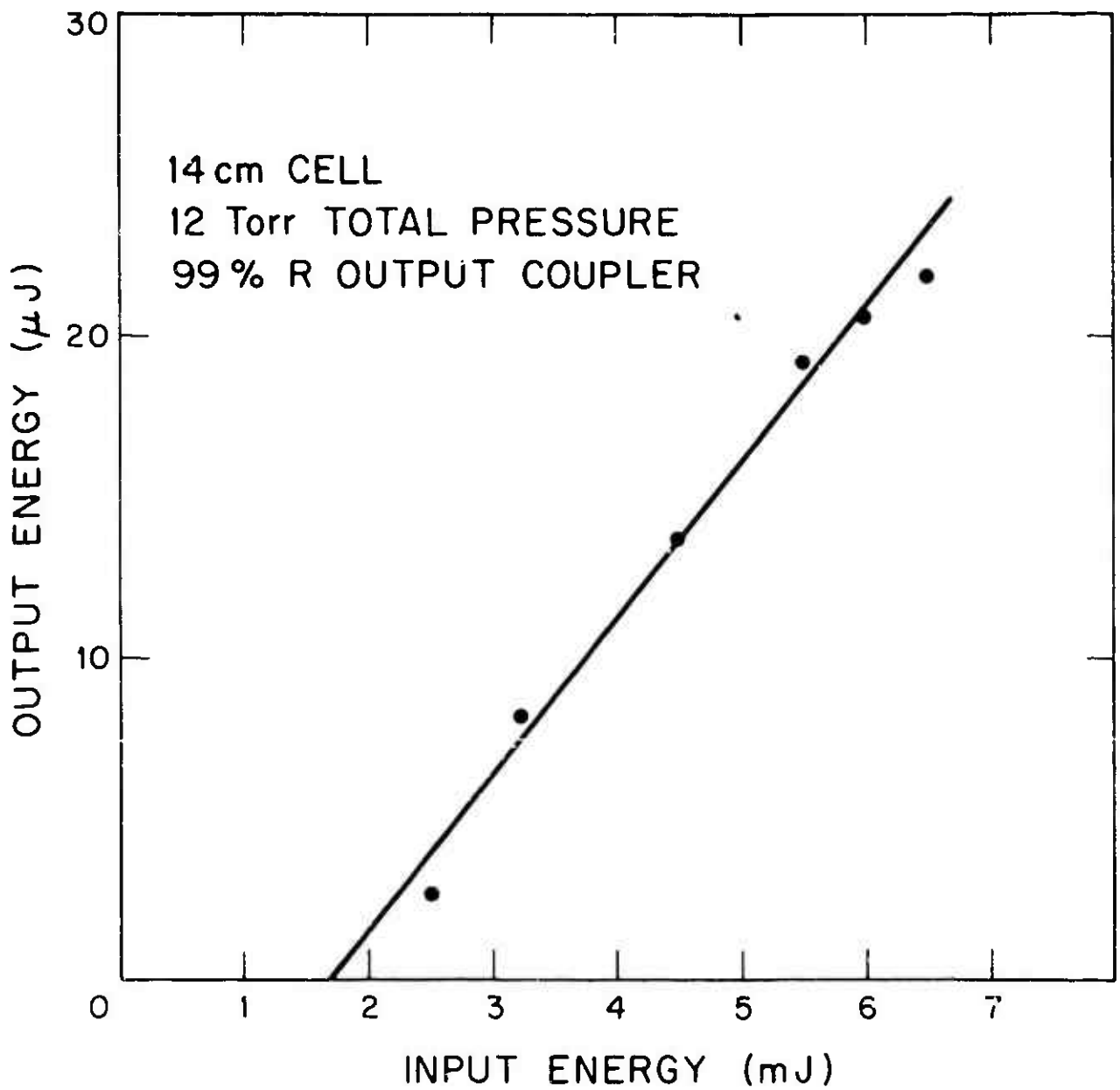
18-8-13241
14 cm CELL
12 Torr TOTAL PRESSURE
99 % R OUTPUT COUPLER
OUTPUT ENERGY (μJ)
INPUT ENERGY (mJ)
0
10
20
30
1
2
3
4
5
6
7

Fig. 3.1-

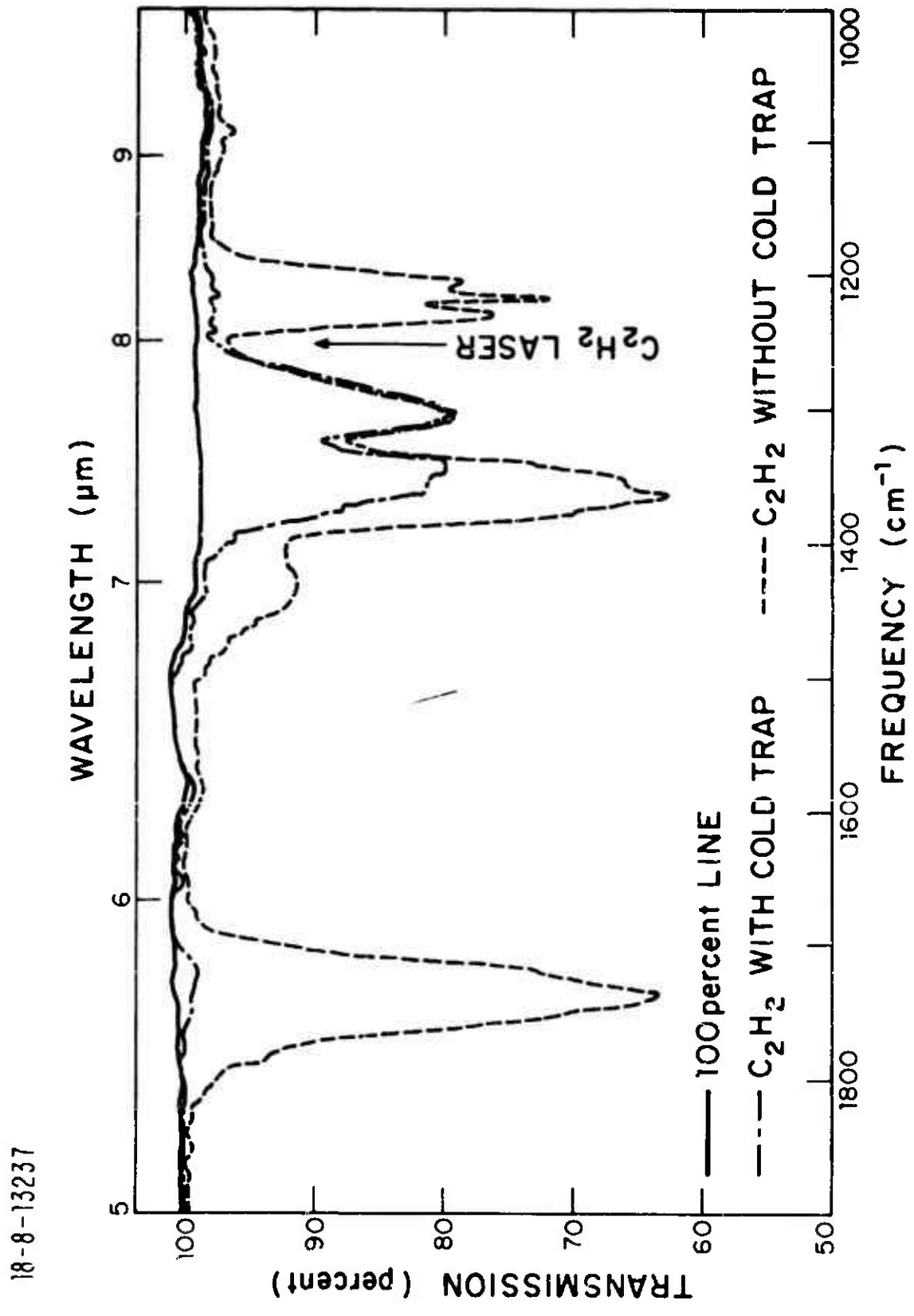
18-8-13237
TRANSMISSION (percent)
100
90
80
70
60
50
WAVELENGTH (μm)
5
6
7
8
9
FREQUENCY (cm⁻¹)
1800
1600
1400
1200
1000
C2H2 LASER
100percent LINE
C2H2 WITH COLD TRAP
C2H2 WITHOUT COLD TRAP

Fig. 3.1-2

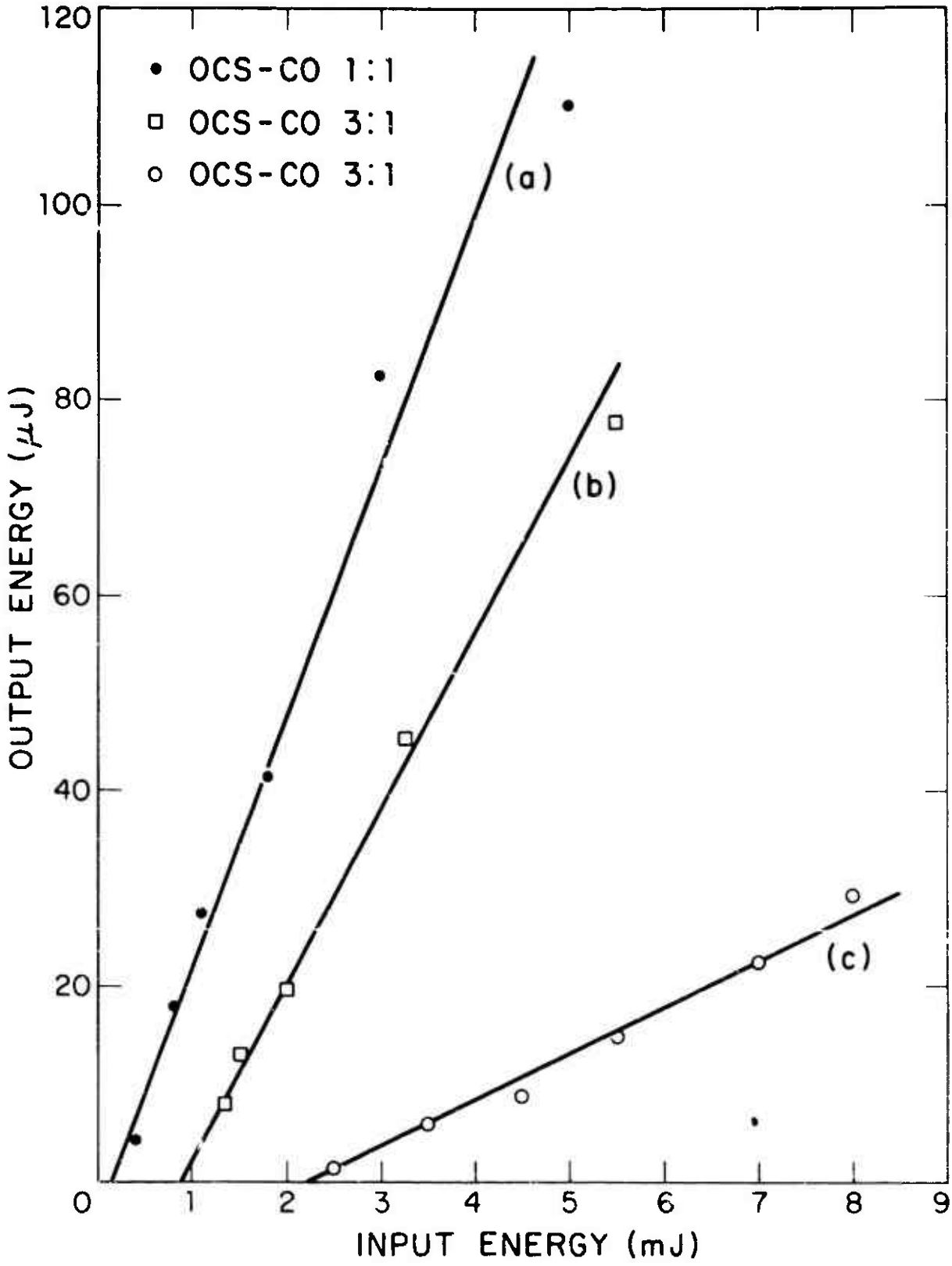
• OCS-CO 1:1
□ OCS-CO 3:1
○ OCS-CO 3:1
(a)
(b)
(c)
OUTPUT ENERGY (μJ)
INPUT ENERGY (mJ)
0
20
40
60
80
100
120
1
2
3
4
5
6
7
8
9

Fig. 3.1-3

18-8-13239

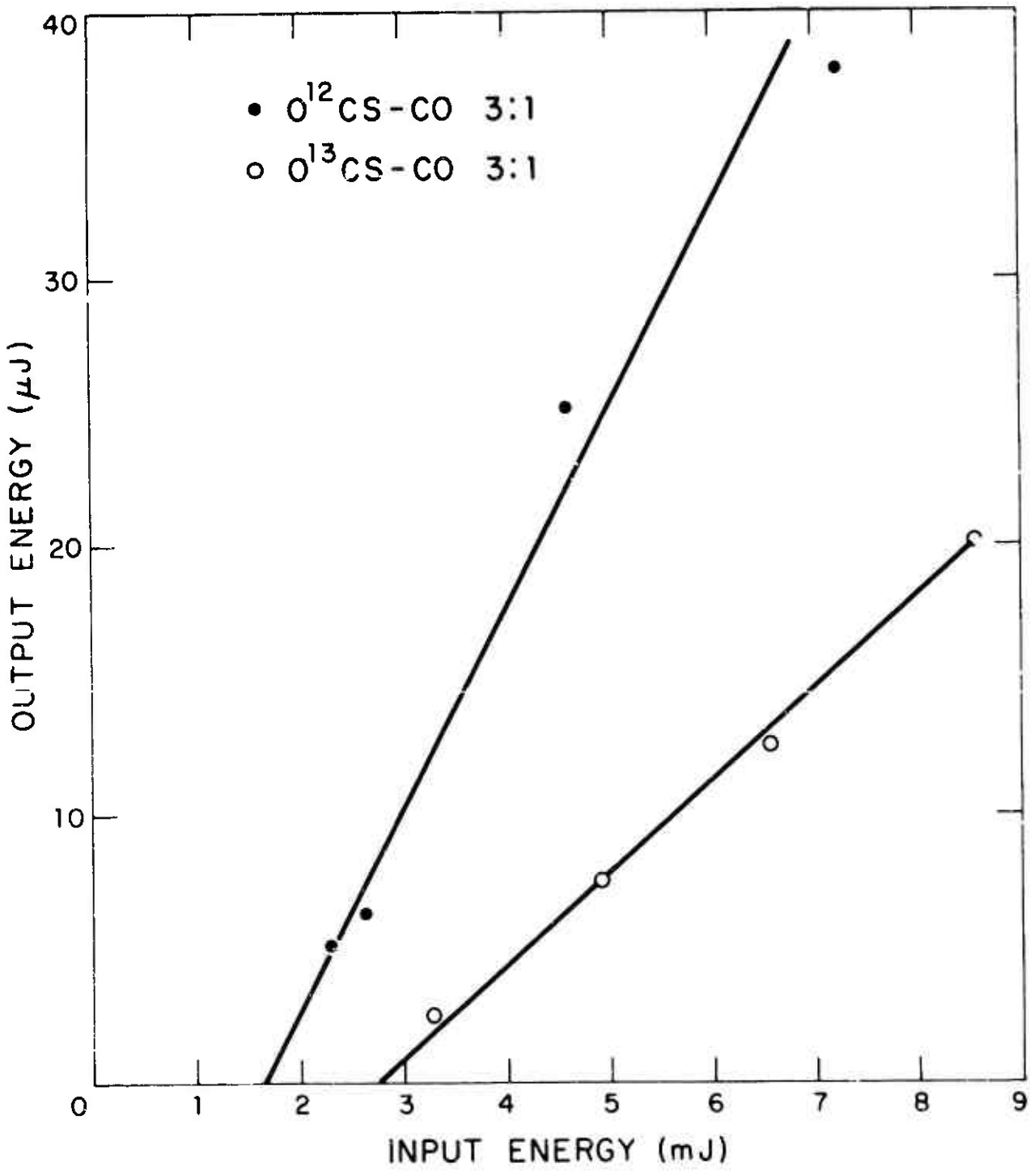

Fig. 3.1-4

18-8-13240

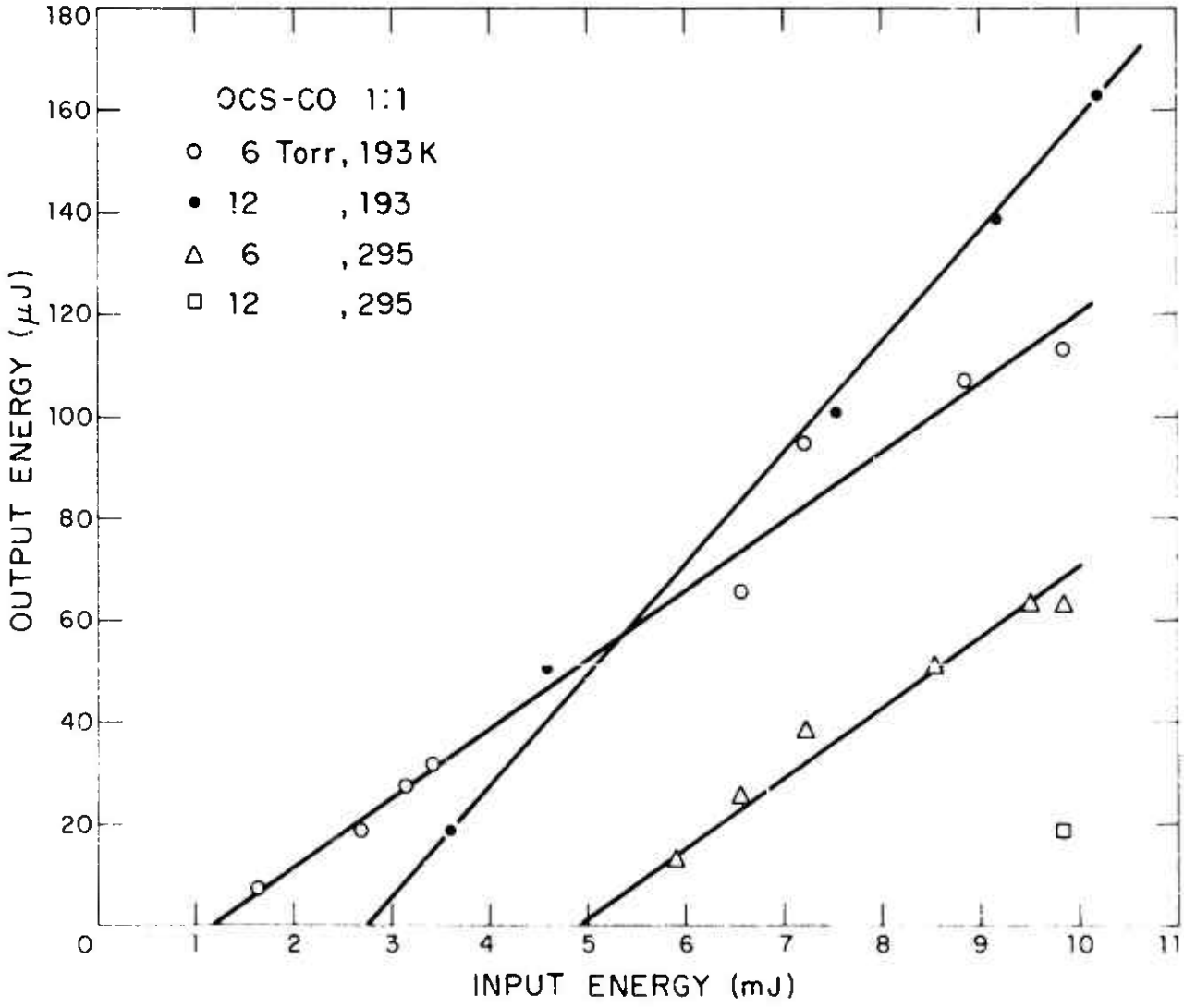

Fig. 3.1-9

Table 3.1-1. Observed vacuum frequencies of the SiH_4 laser (± 0.04 cm^{-1})

Frequency cm^{-1}
1265.50
1262.31
1258.02
1257.10
1254.66
1251.25

Table 3.1-2. Possible tetrahedral molecules for the V-V transfer laser

	$\nu_1(A_1)$	$\nu_2(E)$	$\nu_3(F_2)$	$\nu_4(F_2)$
SiH_4	2187	975	2191	914
GeH_4	2111	931	2112	821
CD_4	2085	1054	2258	996

CO band center is at 2143 cm^{-1}.

Table 3.1-3. Upper pressure limits for the C_2H_2 and the OCS lasers

Laser Medium	Mixture	Cell Length (cm)	Pressure Limit (Torr)
C_2H_2-CO-He	1:1:0	14	46
	1:1:5	4.3	610
	1:3:30	14	395
OCS-CO-He	1:1:0	4.3	115
	1:1:7	4.3	418
	1:1:20	14	390

Table 3.1-4

Observed C_2H_2 laser lines		Calculated frequencies for the 01000-00001[1] Q(J) - branch transitions.			
This Work	Ref. a	J	C_2H_2 (ref. b and c)	C_2HD (ref. b)	C_2D_2 (ref. b)
		1	1245.17	1176.04	1226.11
		2	1245.14	1176.02	1226.09
		3	1245.08	1175.99	1226.06
		4	1245.02	1175.94	1226.02
		5	1244.93	1175.89	1255.97
		6	1244.83	1175.83	1225.91
	1244.70	7	1244.71	1175.75	1225.84
		8	1244.57	1175.67	1225.76
1244.52	1244.46	9	1244.42	1175.57	1225.66
		10	1244.25	1175.46	1225.56
1244.12	1244.09	11	1244.06	1175.34	1225.45
		12	1243.85	1175.22	1225.33
1243.75	1243.64	13	1243.63	1175.08	1225.20
		14	1243.39	1174.93	1225.05
1243.08	1243.12	15	1243.13	1174.77	1224.90
		16	1242.86	1174.60	1224.73
		17	1242.57	1174.42	1224.56
		18	1242.26	1174.23	1224.38
		19	1241.93	1174.03	1224.18
		20	1241.59	1173.82	1223.98

[a] C. F. Shelton and F. T. Byrne, Appl. Phys. Lett. 17, 439 (1970).

[b] H. Fast and H. L. Welsh, J. Mol. Spectrosc. 41, 203 (1972).

[c] J. Pliva, J. Mol. Spectrosc. 44, 145 (1972).

Table 3.1-5. Observed vacuum frequencies of the $O^{13}CS$ laser

Frequency (cm^{-1})
1145.09
1146.41
1148.13
1162.94
1163.63
1164.83

3.2 16 μm CO_2 Laser

Since the last reporting period, we have obtained 16 μm laser oscillation in an optically-pumped mixture of HBr-CO_2. Subsequent to this result, several months were spent in trying to determine the basic physical properties of the laser. Once these were known, improvement in the laser could then proceed in a more logical manner. These early studies are described in detail in a preprint of a journal article (Appendix 3.2-A)which is included at the end of this section.

We may summarize the major result of this study as follows:

i) A total inversion exists for the 16 μm transition and, therefore, P, Q, and R branch operation may all be obtained from the laser.

ii) The characteristic rotational relaxation time is faster than the fastest vibrational relaxation rate (i.e., V-V transfer to the other Fermi mixed level). As a result the laser may be scaled with pressure, as long as the rate of stimulated pumping of the $[10^0 0, 02^0 0]_{II}$ level is also scaled correspondingly.

iii) It is not necessary to cool the CO_2 gas to -80°C to achieve gain on the 16 μm transition. This result was anticipated on the basis of the threshold criteria.

iv) By judicious choice of cavity mirror reflectivities it is possible to operate the laser without a 9.6 μm stimulating pulse. Experimentally this was demonstrated for the analogous 14 μm CO_2 laser.

With these results known, we began work on improving the laser performance. In order to scale the output of the 16 μm laser to a practical level, it is convenient to raise the operating pressure over the 2 to 3 Torr value discussed in the Appendix 3.2-A. Result "ii" above indicates the chief limitation on pressure scaling was the output power (not necessarily energy) of the pulsed CO_2 laser. We, therefore, replaced the CO helical TEA laser with a commercial transverse

discharge laser. Typically this laser produces a single line output energy of 200-300 mjoules in a 200 ns pulse.*

Although at this time this high power laser has been used for only a limited number of experiments we have been able to make significant improvement on the 16 μm laser performance. For example, we are now able to operate the laser repeatably at 100 Torr pressure (5 Torr HBr-CO_2 mixture, 95 Torr Argon buffer). The optimum CO_2-HBr total pressure is now 4 to 5 Torr, as opposed to 2 Torr previously. This pressure is still somewhat lower than the value one would need for total absorbtion of the laser radiation by the gas. Further, improvement in pressure scaling can be expected after changes in cavity geometry, pulse delay, etc. are instituted. Finally, using the new CO_2 laser we have been able to realize room temperature operation of the 16 μm laser. This improvement is not unexpected since 0°C operation was attained with the lower energy laser.

In addition to our work on the HBr-CO_2 optical pumped laser, we have experimentally evaluated the feasibility of other optical pumping schemes to generate wavelengths desirable for LASL applications. Our first area of interest was the use of other hydrogen halide lasers to obtain a 16 μm CO_2 laser completely analogous in principle to that used on the HBr laser. In particular, optical pumping with HF seems a singularly desirable approach.† This point may be argued on the basis of the high energy output available from the HF laser as well as the more developed chemical reactant technology for IR lasers (in comparison to HBr lasers). In order to demonstrate the general applicability of this approach, we converted the HBr pin laser to HF and used it to pump a low pressure sample of CO_2 and HF. The resulting optically pumped laser oscillated strongly at 9.6 μm. Sixteen micrometer output was not seen because the BaF_2 windows on the sample cell, which were resistant

*Compare this to the values of 80 m joules in a 2-3 μs pulse in the helical TEA laser used in the initial research.

†Excitation of a DF-CO_2 mixture with a DF chemical laser seems kinetically more favorable.

to HF, were opaque at 16 μm. Further experiments with DF laser pumping of a DF-CO_2 mixture to obtain a 16 μm laser are anticipated.

We have also used the HBr laser to pump a OCS transfer laser. The kinetics are analogous to that in the CO-OCS system described by Kildal and Deutsch; and thus the operating parameters -- pressure, wavelength are also similar. The chief results of the experiment was to demonstrate further the utility of hydrogen halide optical pumping systems as a technique for generating wavelengths of interest to the LASL isotope separation effort.

Finally, we have examined the existing experimental and theoretical data on the spectroscopy and band strengths of the "16" μm band in other CO_2 isotopes. These data indicate that other isotopes will be suitable for obtaining additional laser wavelengths in the 16 μm region.

R. M. Osgood, Jr.

OPTICALLY PUMPED 16 μm CO_2 LASER*

R. M. Osgood, Jr.
Lincoln Laboratory, Massachusetts Institute of Technology
Lexington, Massachusetts 02173

Abstract

A potentially useful 16 μm CO_2 laser, oscillating on the $[10^0 0, 02^0 0]_{II}$ to $01^1 0$ transition, is described. The $v = 1 \rightarrow v = 0$ lines from an HBr chemical laser were used to pump a low pressure mixture of HBr and CO_2 gases. Vibrational energy transfer from HBr followed by a 9.6 μm stimulating pulse populated the CO_2 $[10^0 0, 02^0 0]_{II}$ level.

*This work was sponsored by the U. S. Energy Research and Development Administration under a subcontract from the Los Alamos Scientific Laboratory.

Given the limited number of strong infrared laser sources, a convenient way of generating secondary sources of reasonable efficiency and power, is by the optical pumping of molecular gases. This may be done either by direct optical excitation of the laser gas,[1] or by optical pumping of a resonant absorber followed by collisional vibrational to vibrational (V-V) energy transfer to the laser gas.[2] The second technique is particularly useful for optical pumping schemes utilizing a hydrogen halide chemical laser as the optical pump. These lasers are known to be both strong and relatively efficient sources in the 2.5 μm to 6 μm wavelength region. In addition, a sizable fraction of the output energy from these lasers is in lines within the $v = 1 \rightarrow v = 0$ vibrational rotational band of the molecule. Thus, the same hydrogen halide gas may be included in the gas mixture to act as the resonant absorber for most of the pumping wavelengths. The collision cross sections for resonant V-V exchange between the first vibrational level in hydrogen halides and high lying vibrational modes in polyatomic molecules are known to be large. In essence, optical pumping with a hydrogen halide chemical laser and the same hydrogen halide as a self absorber is a particularly clean technique for channeling the chemical energy of the hydrogen and halogen reactions into a specific vibrational mode. Many of the undesirable aspects of in situ chemical reactions and energy transfer processes,[3] such as gas heating and relaxation by atomic species or reactants, are not present in the optical pumping approach.

In this letter, we report using such an optical pumping scheme involving hydrogen halides to develop a laser at 16 μm and 14 μm. The former wavelength region is of immediate practical interest because of its potential application to laser separation of uranium isotopes.[4]

The essential physics of the laser inversion process are depicted in Fig. 1. The $v = 1 \rightarrow v = 0$ transitions generated in an HBr chemical laser are used to excite the $v = 1$ level of HBr. Vibrational energy transfer from the HBr populates

the fundamental of the asymmetric stretch mode ($00^0 1$) in CO_2. A strong stimulating field at 9.6 μm (or 10.6 μm) then acts to drive the molecule into the Fermi mixed $[10^0 0,\ 02^0 0]_{II}$ (or $[10^0 0,\ 02^0 0]_I$) level. If 9.6 μm saturation occurs promptly with respect to the rapid collisional deactivation of this level,[5] a population inversion will be formed between the mixed level and the first excited bending mode ($01^1 0$). Since the $01^1 0$ state is only 600 cm^{-1} above the ground vibrational state, it is useful to reduce its thermal population by cooling, thereby minimizing the threshold population requirements of the mixed level.

A schematic of the apparatus is shown in Fig. 2. The HBr laser used discharge production of the reactants, $H + Br_2$, and is similar in design to that described in Ref. 6. It had an output power of 100 mjoules in a 200 nsec pulse, with approximately 2/3 to 1/2 of the total laser power in the desired $v = 1 \rightarrow v = 0$ transitions. A CO_2 pin laser with conventional helical discharge geometry was used to generate the 9.6 μm saturating pulse. The laser had an intra-cavity grating to force oscillation on a selected vibrational-rotational line in the 9.6 μm P-branch. Its output consisted of a, typically, 3 μsec pulse (see Fig. 3a) containing 80 millijoules of energy. Spectral measurements of all laser lines were done with a 1/2 meter Bausch & Lomb monochromator. The Cu:Ge detector and its amplifier had a 1 MHz bandwidth.

The optically-pumped laser cavity (for details see inset Fig. 2) was formed by two dichroic mirrors, both with a 10 m radius of curvature. Mirror one (M1) was 99% reflective at 16 μm, 95% reflective at 14 μm, and 80% transmissive at 4.3 μm. Mirror two (M2) was 98% reflective at 16 μm and 50% transmissive at 9.6 μm. The stainless steel sample cell within the optical cavity could be cooled to -80^0C by means of a closed cycle cooler. The cell required a vacuum box to protect its KBr windows from atmospheric water vapor condensation when the cell was cooled. The 4.1 μm pump radiation was directed into the cavity through M1.

and focused to a 4 mm beam diameter at the center of the cell. Because of the complete saturation of the gas medium by the 9.6 μm pulse, focusing was not necessary for the beam coming from the CO_2 laser through M2.

The pressure range of the HBr-CO_2 mixture for which 16 μm stimulated emission was observed was from 0.5 to 7 Torr. Typically a 50-50 mixture of HBr and CO_2 was optimal. Up to 12 Torr of argon could be added to a 1.5 Torr CO_2-HBr mixture before quenching of the 16 μm emission occurred. As argon was added, the various spectral lines would quench: first R, then P, and finally Q. This order of quenching is consistent with the ordering of gain among the three rotational-vibrational branches if a total inversion exists (see below). To simplify the discussion which follows, we will now confine our attention to only those pressure effects obtained by adding argon to relatively low partial pressures (a few Torr of a 50%-mixture of HBr and CO_2).[8]

Figure 3 shows a typical 9.6 μm pulse (Fig. 3a), and the 16 μm pulse, at two different values of argon partial pressure (Fig. 3b and 3c) in the sample cell. At low cell pressures 3(b), the 16 μm pulse had a duration of a few microseconds. With increasing argon partial pressure, the pulse duration shortened but its peak amplitude increased. At highest pressures, the measured pulse width was 200 nsec, although this measurement may be limited by the frequency response of the detection system. The delay time between the 9.6 μm and 4.1 μm pulses was varied to ascertain its effect on the 16 μm laser output energy. It was found that this energy varied with the delay in a manner consistent with the known collisional dynamics of the $CO_2 00^0 1$ level in a vibrationally excited HBr-CO_2 mixture;[8] i.e., the 16 μm energy increased with delay until V-V transfer was complete and then fell off at a rate equal to the V-T rate of the vibrationally couplex mixture. Finally, the onset of the 16 μm pulse followed the 9.6 μm stimulating pulse by 100-200 nsec, a delay consistent with buildup time in gas lasers of intermediate gain.

Analysis of the spectral output indicated that at optimum pressures the optical-pumped laser would oscillate simultaneously on the P, R, and Q branch lines of the $[10^00, 02^00]_{II}$ to 01^10 band. The relative strengths of these three branches generally depended on the degree to which the laser gain exceeded threshold, and the instantaneous length of the cavity. The fact that both R and Q branches were seen indicates the population inversion is indeed total. Also at low and intermediate pressures (see below for pressure range),it was found that the particular P and R rotational transition which oscillated was the one whose upper rotational level corresponded to the lower rotational level of the 9.6 μm transition. At higher pressures, transitions appeared which were unconnected to the lower level of the 9.6 μm transition but which fell closer to the peak of the thermalized rotational distribution.

The results presented above can be satisfactorily explained by considering the interplay between the rates of stimulated emission on the 9.6 μm band, rotational relaxation, and the fastest vibrational relaxation – i.e., the decay of the $[10^00, 02^00]_{II}$ level to the two other near resonant vibrational levels. Although a detailed quantitative model of these collisional processes can not be presented here, its qualitative features are as follows.[9] For the low range of the pressures used here, the rate of stimulated emission greatly exceeds the rotational and vibrational relaxation rates. Further, the 9.6 μm laser pulse width is of the same duration as the time for complete rotational relaxation of the rotational manifold.[10] Under these conditions,and if the J of the 9.6 μm stimulated transition is not far from the peak of the thermalized rotational distribution, the line of highest gain in the P, Q, and R branch throughout the duration of the pump pulse will remain that line with the upper rotational level identical to the terminal level of the 9.6 μm transition. Also for low pressures, the 16 μm pulse length will be comparable to the CO_2 pulse length ~ several microseconds. This behavior results from the fact that as long as rotational thermalization of the entire rotational manifold is

incomplete, the rotational levels not experiencing stimulated pumping act as a reservoir and a sink for the upper and lower laser levels, respectively; thus, a 16 μm inversion will persist as long as 9.6 μm pump field is on. At higher pressures, the rotational thermalization occurs on a much shorter time scale than the stimulating pulse. As a result, the 16 μm pulse is much shorter than the 9.6 μm pump pulse, but the total energy of the pulse is the same. This is in accord with Figs. 3b and c. Further, it can also be shown that under these conditions, the rotational level of highest gain does not remain the pumped level throughout the 9.6 μm pulse, but will in fact switch to a level near the maximum of the Boltzmann distribution. This result is also in accord with spectral observations. Finally, at the highest pressures the relaxation rate to the other near resonant vibrational levels becomes fast compared to 16 μm pulse buildup time, and this effect reduces the total time averaged gain to below threshold.

Experiments with the 14 μm laser were limited to confirming that laser oscillation could be obtained without the use of an externally applied stimulating pulse. Instead, the 10.6 μm pulse was generated internally within the same cavity as the 14 μm emission. This was accomplished by using the same techniques; cooling, gas mixtures, etc., as in the 16 μm laser, except that now mirror M2 was replaced by a gold 50 cm radius of curvature mirror. With this relatively lossy cavity at 10.6 μm (M1 was 40-50% reflective at 10.6 μm), the pulse formation time at 10.6 μm was delayed until a large population was transferred into the $00^0 1$ level. Under these conditions, the 10.6 μm induced population of the $(10^0 0,\ 02^0 0)_I$ was sufficiently abrupt compared to the vibrational relaxation that the transient gain on the 14 μm level exceeded threshold. If, on the other hand, M1 was replaced by a 99% reflector at 10.6 μm, virtually no hold-off of the formation of the 10.6 μm pulse occurred. Thus a large transient population was never formed and the 14 μm gain never exceeded threshold.

In summary, we have demonstrated the usefulness of optical pumping with a hydrogen halide laser to achieve laser action in a wavelength region of practical

interest. Improvement in laser performance may be anticipated through the use of other hydrogen halide systems (HCl and DF, for example);[11] and by straightforward optimization of the cell length, laser optics, and CO_2 laser pump pulse length. Experiments to effect such an optimization and to measure the laser output energy and efficiency are now being undertaken.

Finally, I would like to thank the members of the Quantum Electronics Group at Lincoln Laboratory for their useful comments and discussions and to thank A. Szöke, H. Schlossberg, S. Marcus, and B. Feldman for much enlightenment. Also special appreciation is extended to D. Sullivan for his dedicated technical help.

REFERENCES

1. N. Skribanowitz, I. P. Herman, and M. S. Feld, Appl. Phys. Lett. 21, 466 (1972); T. Y. Chang and O. R. Wood, Appl. Phys. Lett. 23, 370 (1972); H. R. Schlossberg and H. R. Fetterman, Appl. Phys. Lett. 26, 316 (1975).
2. T. Y. Chang and O. R. Wood, Appl. Phys. Lett. 24, 182 (1974); H. Kildal and T. F. Deutsch, Appl. Phys. Lett. 27, 500 (1975).
3. H. L. Chen, J. C. Stephenson, and C. B. Moore, Chem. Phys. Lett. 2, 593 (1968).
4. P. Robinson, Proceedings of New York Academy of Science, April 1975, (to be published).
5. An excellent summary of the kinetics and spectroscopy involved in a 16 μm CO_2 laser are given by O. P. Judd in Los Alamos Report LA-5892-MS, February, 1975.
6. O. R. Wood and T. Y. Chang, Appl. Phys. Lett. 20, 69 (1972); I. Burak, Y. Noter, A. M. Ronn, and A. Szöke, Chem. Phys. Lett. 13, 322 (1972).
7. The gas temperature for all work described here was near $-80^{o}C$. However, depending on the degree to which the laser was pumped above threshold higher gas temperatures could be tolerated. The warmest value for which laser oscillation was observed was $0^{o}C$.
8. J. C. Stephenson, J. Finzi, and C. B. Moore, J. Chem. Phys. 56, 5214, (1972).
9. A. L. Golger, and V. S. Letokhov, Sov. J. Quantum Elec. 3, 428 (1974). This article mathematically treats the interactions of stimulated excitation, rotational relaxation, and vibrational relaxation in essentially similar optical pumping schemes.
10. G. T. Schappert, Appl. Phys. Lett. 23, 319 (1973).
11. In order to show the feasibility of using DF optical pumping, we have recently obtained laser action at 10.6 μm in a HF optically-pumped mixture of HF-CO_2.

FIGURE CAPTIONS

Fig. 1. Simplified vibrational energy level diagram of CO_2 and HBr which summarizes physical processes involved in 16 μm and 14 μm CO_2 laser.

Fig. 2. Schematic of apparatus used to optically-pump HBr-CO_2 gas mixture.

Fig. 3. A typical 9.6 μm laser pulse (a) 2 μsec/large division); and the 16 μm laser pulse at two different values of argon pressure (b and c, 500 ns/large division). The argon partial pressures for b and c are 0 and 3 Torr respectively; the HBr-CO_2 partial pressure was 1.5 Torr for both b and c. The vertical sensitivity is the same in b and c.

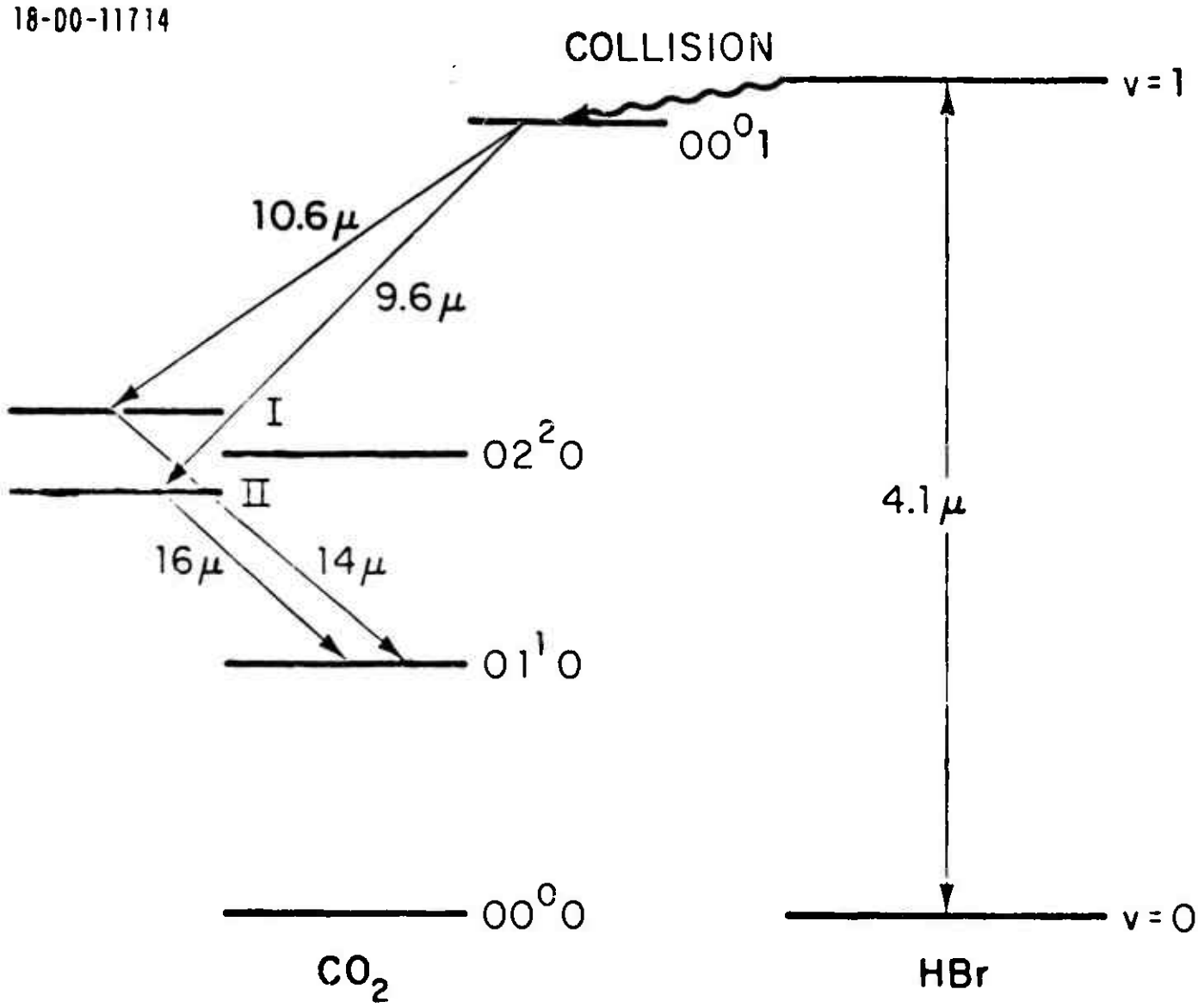
18-DO-11714
COLLISION
v = 1
$00^0 1$
10.6μ
9.6μ
I
$02^2 0$
II
4.1μ
16μ
14μ
$01^1 0$
$00^0 0$
v = 0
CO_2
HBr

Fig. 3.2-

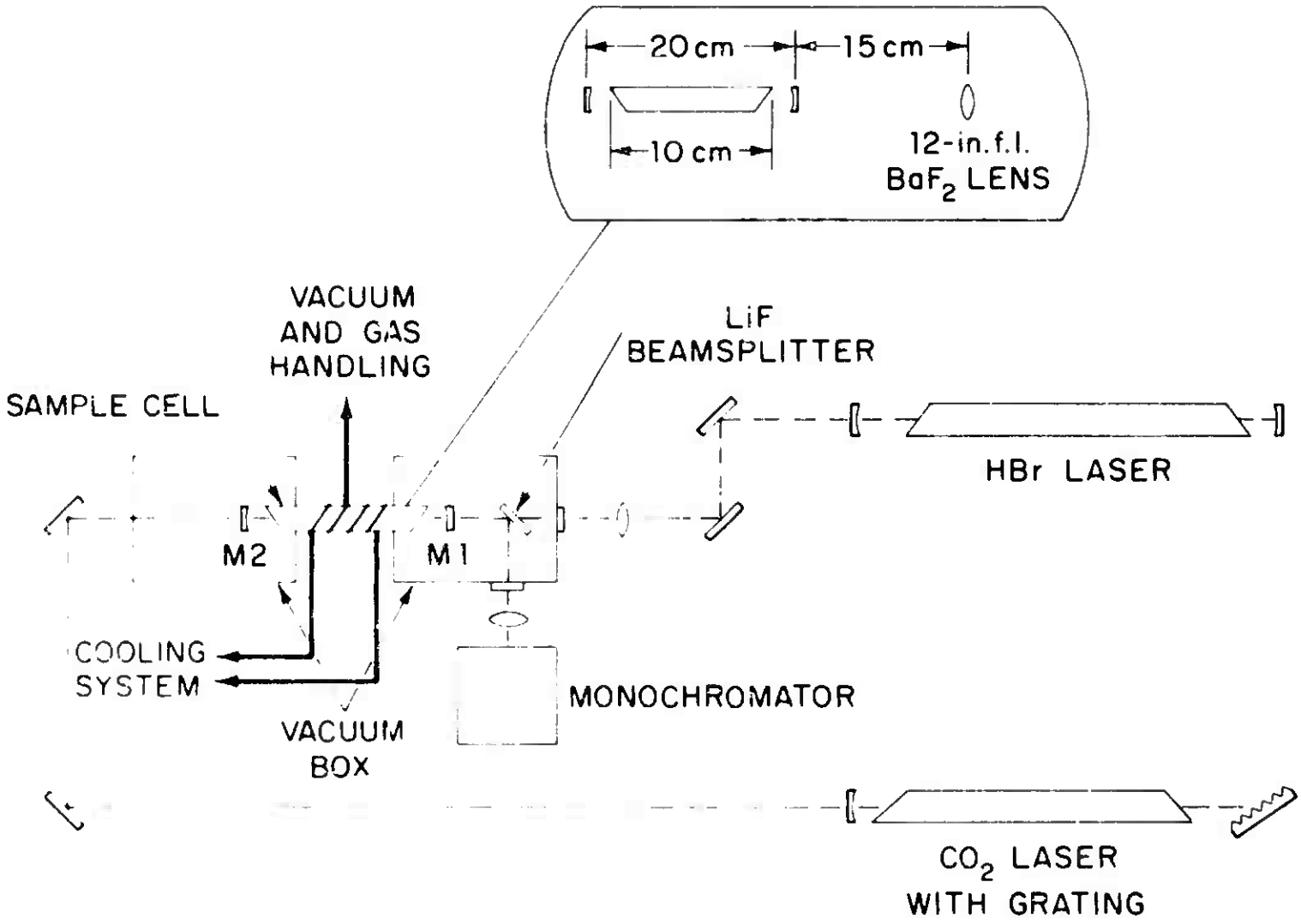
20 cm
15 cm
10 cm
12-in.f.l.
BaF2 LENS
VACUUM
AND GAS
HANDLING
LiF
BEAMSPLITTER
SAMPLE CELL
HBr LASER
M2
M1
COOLING
SYSTEM
MONOCHROMATOR
VACUUM
BOX
CO2 LASER
WITH GRATING

Fig. 3.2-2

-DO-11739

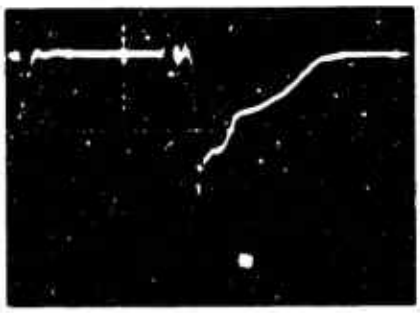

(a)

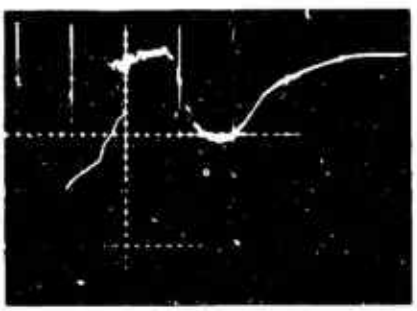

(b)

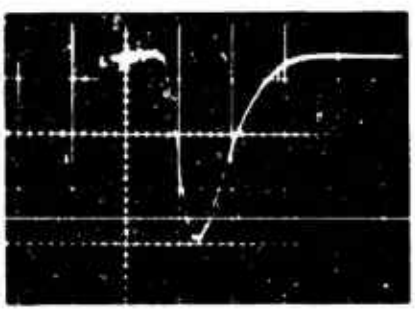

(c)

Fig. 3. 2-3

4. CO_2 LASER DEVELOPMENT AND EVALUATION

4.1. 12.2 μm Wavelength Calibration

Using a tunable diode laser we have observed a number of $^{14}NH_3$ and $^{15}NH_3$ absorption lines usable for 12.2 μm wavelength calibration. Some of these lines are also observed on the spectral scan data recently obtained from LASL. In addition, we have precisely measured the frequency difference between the 00^01 - $[10^00, 02^00]_I$ band P(48) transition of a $^{14}C^{16}O_2$ laser and the nearest strong $^{14}NH_3$ absorption line by using direct heterodyne techniques.

Figure 4.1-1 illustrates the experimental arrangement used in our measurements. The outputs of a tunable diode laser and a $^{14}C^{16}O_2$ laser were combined by a beam splitter. One half of the combined radiation was heterodyned on a fast HgCdTe varactor photodiode,[4.1-1] and the beatnote displayed and measured by a microwave spectrum analyzer. The other half of the combined laser radiation was used to probe either of two 1 meter long, 2 cm diameter ammonia cells and the wavelengths of the absorption lines were determined by a 1 meter Spex grating monochromator. Pressures of 2 and 5 Torr were used to fill the $^{15}NH_3$ and $^{14}NH_3$ absorption cells.

The unpublished ammonia data sent to us by Professor K. N. Rao of Ohio State University proved to be of great help in carrying out our experiments. In Figures 4.1-2 and 4.1-3 we reproduce those portions of Rao's ammonia absorption data which we carefully explored for calibrating the 12.2 μm wavelength region. Determination of the calibration lines on the LASL spectral data have been reported separately to LASL.

Careful analysis of either the high resolution LASL measurements (with etalon-related frequency calibration) or our tunable diode laser spectroscopy indicates that some of the absorption features on the Rao data may not be

adequately resolved. For instance, on the LASL spectral scan for $^{15}NH_3$ the etalon shows a 0.05 cm^{-1} spacing for lines #40 and #41, while Fig. 4.1-2 indicates a separation of 0.114 cm^{-1}. In the $^{14}NH_3$ data of Fig. 4.1-3, line #383 1/2 indicates a feature clearly resolved by tunable laser spectroscopy, but not shown in Rao's tables. Figure 4.1-4 shows a heterodyne beat note of 7,775 $\pm$ 50 MHz between the $^{14}C^{16}O_2$ laser 00^01 - $[10^00, 02^00]_1$ band P(48) transition and the diode laser tuned to the $^{14}NH_3$ ammonia 823.9425 cm^{-1} absorption line (HP line #385 in the data provided by Dr. K. N. Rao) shown in Fig. 4.1-3. Application of the 823.9425 cm^{-1} ammonia line as a reference will place the $^{14}C^{16}O_2$ laser 00^01 - $[10^00, 02^00]_1$ band P(48) emission to 824.1683 cm^{-1}, i.e., 0.11 cm^{-1} higher frequency than previously indicated by our spectrometer data based on $^{12}C^{16}O_2$ calibration.

C. Freed

K. Nill*

REFERENCES

4.1-1 D. L. Spears and C. Freed, "HgCdTe Varactor Photodiode Detection of CW CO_2 Laser Beats Beyond 60 GHz," Appl. Phys. Lett. 23, 445 (1973).

*Laser Analytics Inc.

FIGURE CAPTIONS

Fig. 4.1-1 Experimental set-up for 12 μm wavelength calibration.

Fig. 4.1-2 Observed wavenumbers and identified transitions of the ν_2 band of $^{15}NH_3$ (from K. N. Rao of Ohio State University).

Fig. 4.1-3 Observed wavenumbers and identified transitions of the ν_2 band of $^{14}NH_3$ (from K. N. Rao of Ohio State University).

Fig. 4.1-4 7,775 ± 50 MHz beat note of a $^{14}C^{16}O_2$ laser $00^0 1$ - $[10^0 0, 02^0 0]_I$ band P(48) transition and a diode laser tuned to the $^{14}NH_3$ ammonia 823.9425 cm^{-1} absorption line (H.P. line #385 in the data provided by Dr. K. N. Rao.) Vertical scale: linear, Horizontal scale: 10 MHz/cm.

4.2 High Repetition Rate Q-Switched CO_2 Lasers

The passively Q-switched laser, shown in Fig. 4.2-1 is a modification of the stable, sealed-off cw lasers previously reported. Laser line selection is accomplished by means of a diffraction grating as one of the cavity end reflectors. In addition, the Q-switching version incorporates an intra-cavity stainless steel cell which contains a saturable absorbing gas. The saturable absorber which we have used to the present time is sulfur hexafluoride (SF_6) diluted with helium. This mixture has been demonstrated to be an efficient Q-switcher of the high-gain lines in the P-branch of the 10.6 μm band.[4.2-1] The purpose of the helium diluent is to regulate the recovery time of the SF_6 absorber and consequently the PRF of the laser. Typical partial pressures are 0.01 Torr SF_6 and 5 Torr helium.

Figure 4.2-2 shows a passively Q-switched pulse train with a PRF of slightly greater than 100 kHz as well as an individual pulse. For this mode of operation the average power output was 5.5 watts.

By adjusting the helium pressure, the PRF could be varied over a considerable range, with frequencies in excess of 150 kHz observed. This PRF is to our knowledge the highest reported for a passively Q-switched CO_2 laser. As shown in Fig. 4.2-3, however, operating at very high PRF's results in a substantial increase in pulse width. This is due to the fact that the laser gain does not recover completely between pulses and therefore requires a longer time to saturate the SF_6, thus broadening the pulse.

At lower repetition rates, higher peak powers and shorter pulse durations were obtained, as exemplified by the 300 nanosec pulse at 12 kHz PRF in Fig. 4.2-3

As yet, only P(20) of the 10.6 μm band has been studied. Many other lines of both normal and isotopic CO_2 may be Q-switched using SF_6, as well as other absorbing gases.

C. Freed

S. Marcus*

REFERENCES

4.2-1 O. R. Wood and S. E. Schwarz, Appl. Phys. Lett. 11, 88 (1967).

FIGURE CAPTIONS

Fig. 4.2-1 Passively Q-switched stable CO_2 laser.

Fig. 4.2-2 Passively Q-switched CO_2 laser pulse train with 100 kHz repetition rate.

Fig. 4.2-3 Passively Q-switched CO_2 laser pulse shapes at 12 kHz, 40 kHz and 140 kHz repetition rates.

*This work was sponsored by the Department of the Air Force.

12.2 μm WAVELENGTH CALIBRATION

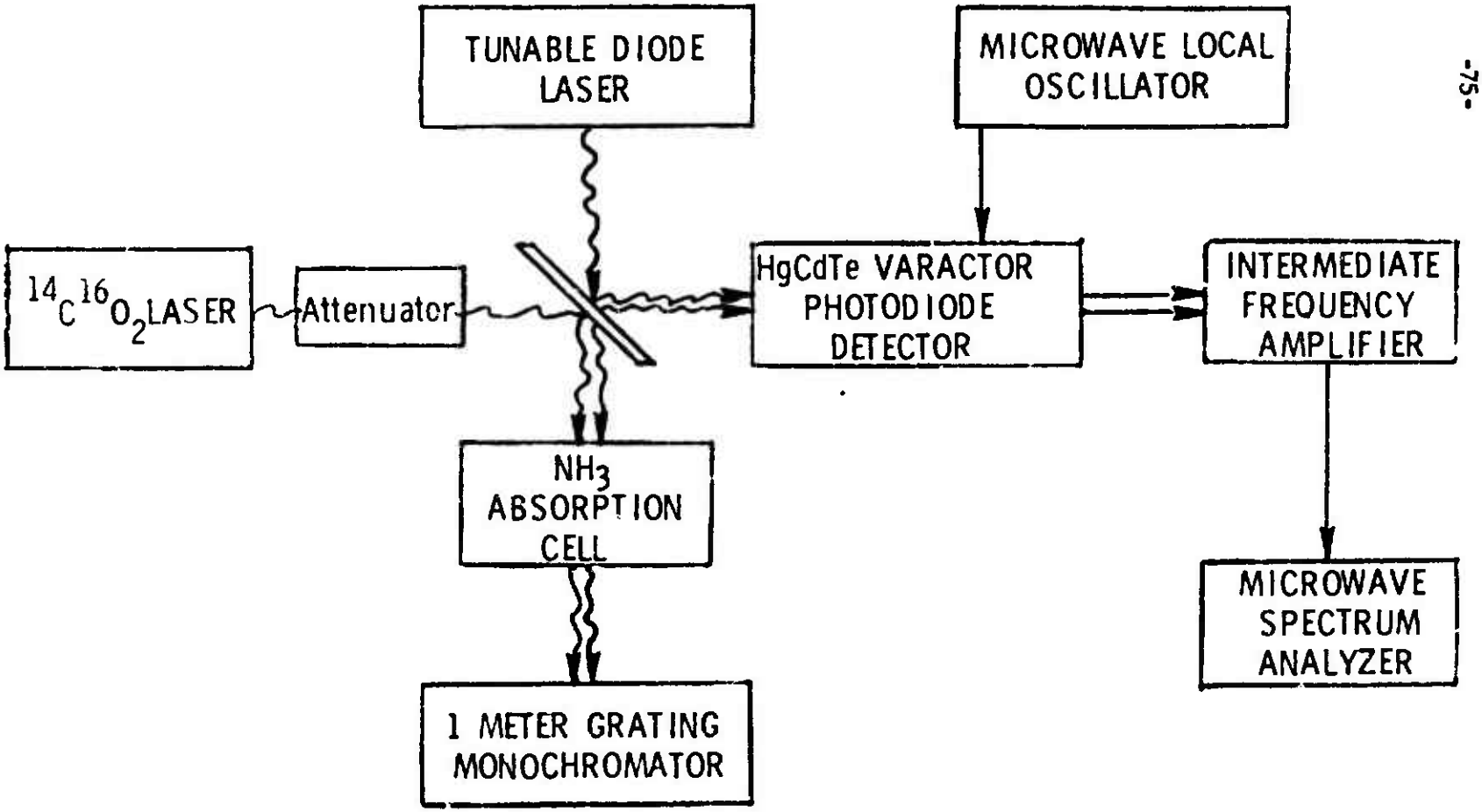

Fig. 4.1-1

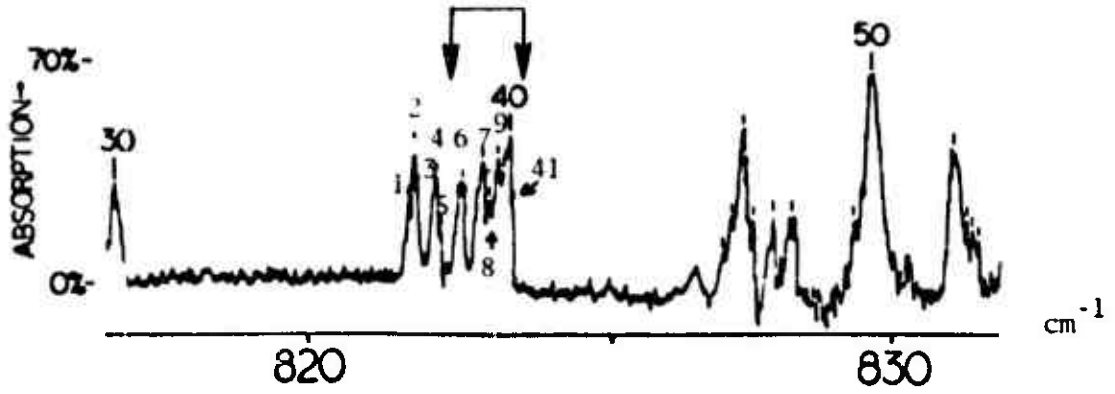

Line No.	Observed Wavenumber (Vac. cm^{-1})	Transition
036	822.452	sP(7,4)
037	822.777	sP(7,3)
038	822.908	sP(7,2)
039	823.025	sP(7,1)
040	823.176	sP(7,0)
041	823.290	

OBSERVED WAVENUMBERS AND IDENTIFIED TRANSITIONS OF THE ν_2 BAND OF $^{15}NH_3$ (K. N. Rao)

Fig. 4.1-2

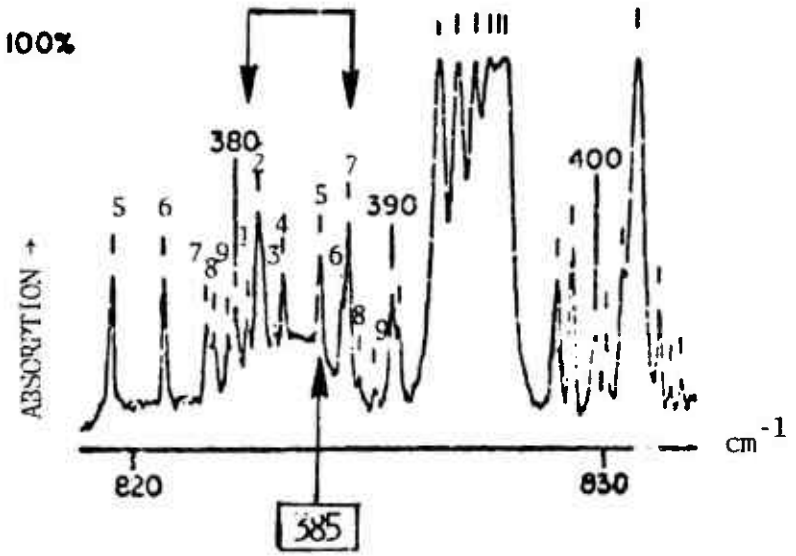

HP Line	LP Line	Observed	Identification
381		822.4381	
382	47	822.6549	2sP(6,3)
383		823.0122	
383 1/2		823.1303	
384		823.1894	
385		823.9425	
386		824.4038	

OBSERVED WAVENUMBERS AND IDENTIFIED TRANSITIONS OF THE ν_2 BAND OF $^{14}NH_3$ (K. N. Rao)

Fig. 4.1-3

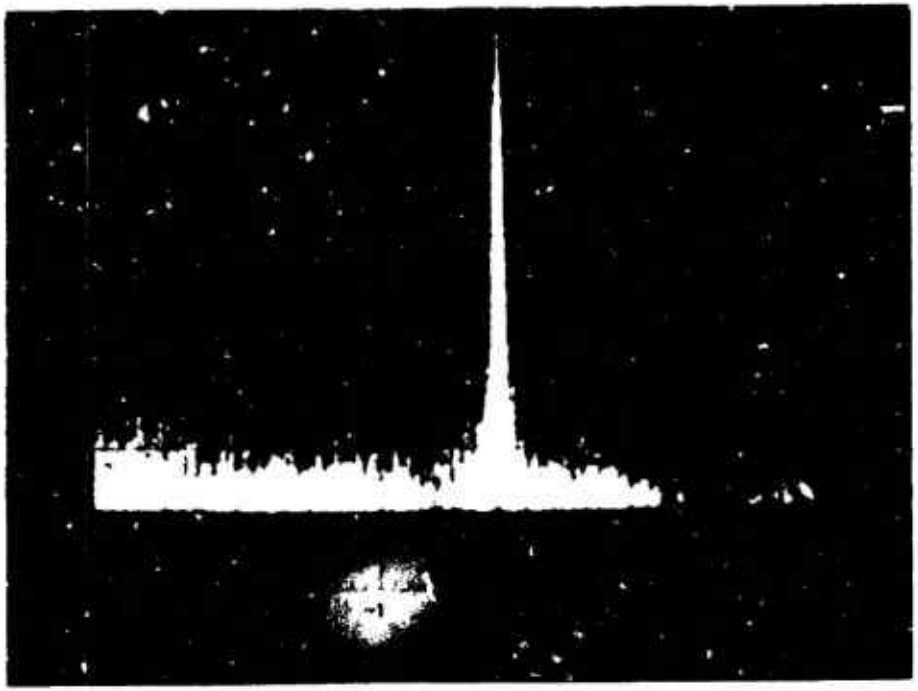

7,775 ± 50 MHz beat note of a $^{14}C^{16}O_2$ laser $00^01 - [10^00, 02^001]_1$ band P(48) transition and a diode laser tuned to the $^{14}NH_3$ ammonia 823.9425 cm^{-1} absorption line (H.P. line #385 in the data provided by Dr. K. N. Rao.)

Vertical scale: linear
Horizontal scale: 10 MHz/cm

Fig. 4.1-4

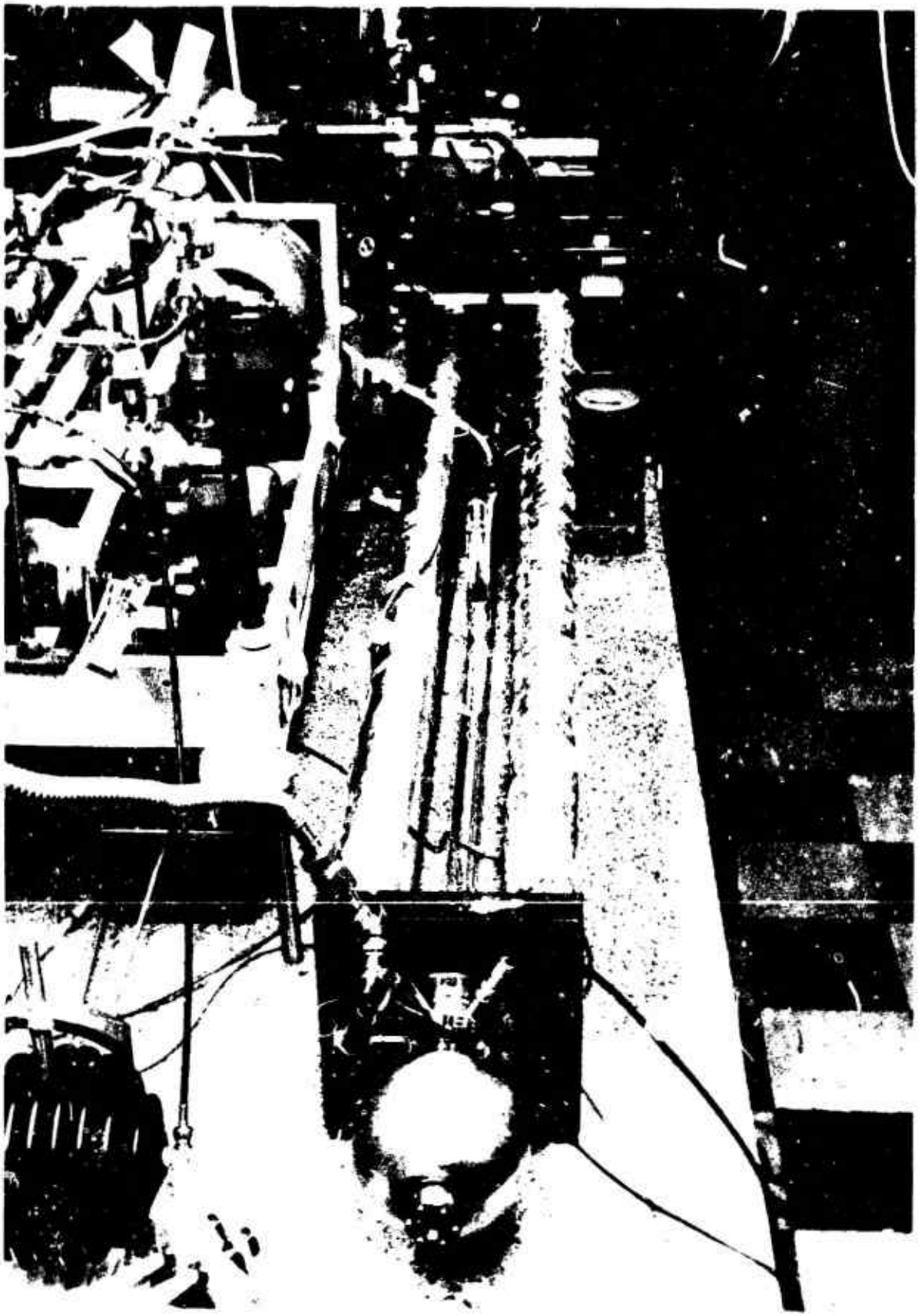

Fig. 4.1-5

-5-6725

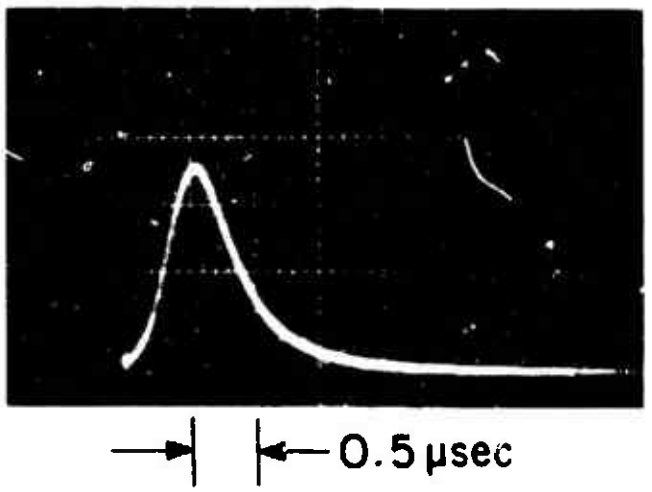

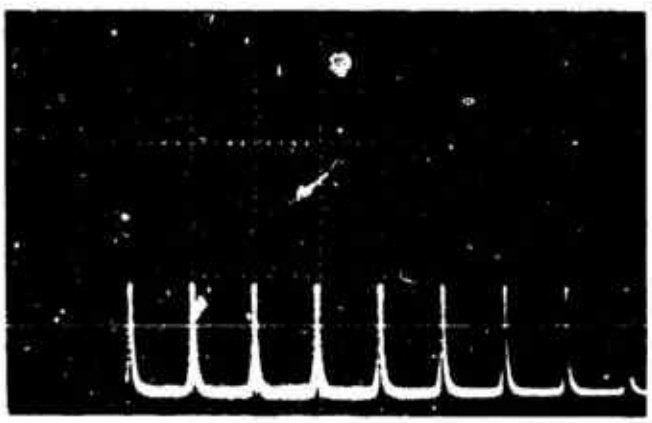

PASSIVELY Q-SWITCHED LASER PULSES

Fig. 4.1-6

-5-6724

PRF = 12 kHz

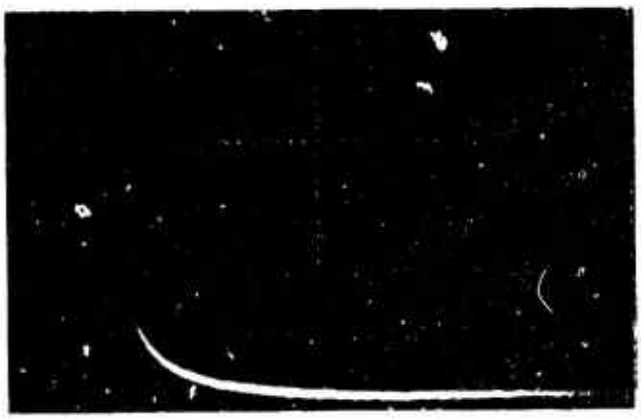

PRF = 40 kHz

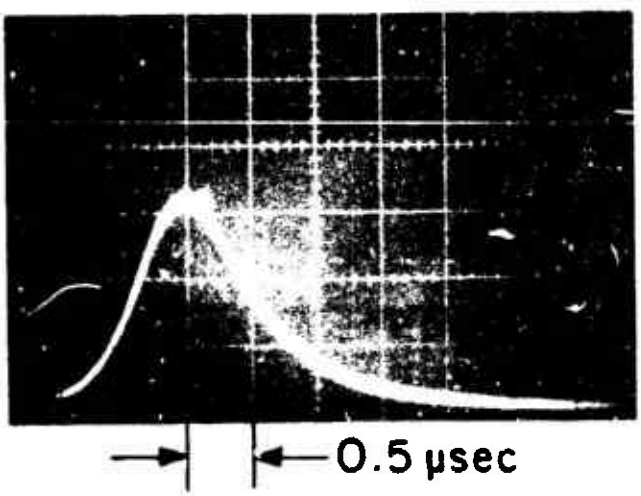

PRF = 140 kHz

PASSIVELY Q-SWITCHED PULSE SHAPES

Fig. 4.1-7

UNCLASSIFIED

SECURITY CLASSIFICATION OF THIS PAGE (When Data Entered)

REPORT DOCUMENTATION PAGE		READ INSTRUCTIONS BEFORE COMPLETING FORM
1. REPORT NUMBER ESD-TR-75-337	2. GOVT ACCESSION NO	3. RECIPIENT'S CATALOG NUMBER
4. TITLE (and Subtitle) Program in Support of the JUMPer Program for Laser Isotope Separation		5. TYPE OF REPORT & PERIOD COVERED Semiannual Report 1 July - 31 December 1975 6. PERFORMING ORG. REPORT NUMBER
7. AUTHOR(s) McWhorter, Alan L.		8. CONTRACT OR GRANT NUMBER(s) F19628-76-C-0002
9. PERFORMING ORGANIZATION NAME AND ADDRESS Lincoln Laboratory, M.I.T. P.O. Box 73 Lexington, MA 02173		10. PROGRAM ELEMENT, PROJECT, TASK AREA & WORK UNIT NUMBERS Project No. 9201
11. CONTROLLING OFFICE NAME AND ADDRESS Air Force Systems Command, USAF Andrews AFB Washington, DC 20331		12. REPORT DATE 31 December 1975 13. NUMBER OF PAGES 88
14. MONITORING AGENCY NAME & ADDRESS (if different from Controlling Office) Electronic Systems Division Hanscom AFB Bedford, MA 01731		15. SECURITY CLASS. (of this report) Unclassified 15a. DECLASSIFICATION DOWNGRADING SCHEDULE

16. DISTRIBUTION STATEMENT (of this Report)

Approved for public release; distribution unlimited.

17. DISTRIBUTION STATEMENT (of the abstract entered in Block 20, if different from Report)

18. SUPPLEMENTARY NOTES

None

19. KEY WORDS (Continue on reverse side if necessary and identify by block number)

JUMPer Program	optical crystals	CO_2 laser
laser isotopes	gas laser research	infrared nonlinear crystal

20. ABSTRACT (Continue on reverse side if necessary and identify by block number)

This report covers in detail the research and development work carried out by M. I. T. Lincoln Laboratory for the U. S. Energy Research and Development Administration under subcontract from the Los Alamos Scientific Laboratory as part of the JUMPer program during the period 1 July through 31 December 1975. The topics covered include infrared nonlinear crystal growth, evaluation, and application; optically pumped gas laser research; and stable CO_2 laser development.

DD FORM 1 JAN 73 1473 EDITION OF 1 NOV 65 IS OBSOLETE

UNCLASSIFIED

SECURITY CLASSIFICATION OF THIS PAGE (When Data Entered)